Infectious Entry of Merkel Cell Polyomavirus

Miriam Becker[1,2], Melissa Dominguez[1,2], Lilo Greune[2,3], Laura Soria-Martinez[1,2,4], Moritz M. Pfleiderer[4,5], Rachel Schowalter[6], Christopher B. Buck[6], Bärbel S. Blaum[4,5], M. Alexander Schmidt[2,3] and Mario Schelhaas*[1,2,4]

[1]Institute of Cellular Virology, ZMBE, University of Münster, Germany

[2]Cluster of Excellence EXC1003, Cells in Motion, CiM, Münster, Germany

[3]Institute of Infectiology, ZMBE, University of Münster, Germany

[4]Research Group, FOR2327 “ViroCarb”, Coordinating University of Tübingen, Germany

[5]Interfaculty Institute of Biochemistry (IFIB), University of Tübingen, Germany

[6]Center for Cancer Research, National Cancer Institute, Bethesda, MD, USA

Running title: MCPyV entry into host cells

Key words: polyomavirus, MCPyV, virus entry, virus-host interaction, endocytosis

Abstract

Merkel Cell Polyomavirus (MCPyV) is a small, non-enveloped tumor virus associated with an aggressive form of skin cancer, the Merkel cell carcinoma (MCC). MCPyV infections are highly prevalent in the human population with MCPyV virions being continuously shed from human skin. However, the precise host cell tropism(s) of MCPyV remains unclear: MCPyV is able to replicate within a subset of dermal fibroblasts, but MCPyV DNA has also been detected in a variety of other tissues. However, MCPyV appears different from other polyomaviruses as it requires sulfated polysaccharides such as heparan sulfates and/or chondroitin sulfates for initial attachment. Like other polyomaviruses, MCPyV engages sialic acid as a (co-)receptor. To explore the infectious entry process of MCPyV, we analyzed the cell biological determinants of MCPyV entry into A549 cells, a highly transducible lung carcinoma cell line, in comparison to well-studied simian virus 40 and a number of other viruses. Our results indicate that MCPyV enters cells via caveolar/lipid raft-mediated endocytosis but not macropinocytosis, clathrin-mediated endocytosis or glycosphingolipid-enriched carriers. The viruses internalized in small endocytic pits that led the virus to endosomes and from there to the endoplasmic reticulum (ER). Similar to other polyomaviruses, trafficking required microtubular transport, acidification of endosomes, and a functional redox environment. To our surprise, the virus was found to acquire a membrane envelope within endosomes, a phenomenon not reported for other viruses. Only minor amounts of viruses reached the ER, while the majority was retained in endosomal compartments suggesting that endosome-to-ER trafficking is a bottleneck during infectious entry.

Importance

MCPyV is the first polyomavirus directly implicated in the development of an aggressive human cancer, the Merkel Cell Carcinoma (MCC). Although MCPyV is constantly shed from healthy skin, MCC incidence increases among aging and immunocompromised individuals. To date, the events connecting initial MCPyV infection and subsequent transformation still remain elusive. MCPyV differs from other known polyomaviruses concerning its cell tropism, entry receptor requirements, and infection kinetics. In this study, we examined the cellular requirements for endocytic entry as well as the subcellular localization of incoming virus particles. A thorough understanding of the determinants of the infectious entry pathway and the specific biological niche will benefit prevention of virus-derived cancers such as MCC.

Introduction

Polyomaviruses (PyV) are small, non-enveloped dsDNA viruses with a diameter of 45-50 nm. The icosahedral (T=7) capids consist of 72 homopentameric capsomers of the major capid protein VP1 with minor capsid proteins VP2/VP3 located within a cavity underneath the VP1 pentamers. The PyV capsid harbors a chromatinized, circular dsDNA genome of about 5 kb (1, 2). Well-studied PyV such as simian virus 40 (SV40), and murine PyV (mPyV) possess a broad cell tropism and can transform cells *in vitro* and in animals (3, 4). Of the human polyomaviruses, JC and BK virus are the best studied (5, 6). JC and BK viruses were initially identified in brain and urine samples, respectively (7, 8). Initial infection with these viruses occurs early in life and typically leads to persistent infections that are typically benign (9-11). Upon immunosuppression, however, persistent JC and BK virus infections may lead to severe diseases, such as progressive multifocal leukoencephalopathy or PyV-associated nephropathy, with potentially fatal outcomes (3, 4).

In 2008, Feng and colleagues identified Merkel cell polyomavirus (MCPyV) in a rare form of skin cancer known as Merkel cell carcinoma (MCC) (12). MCC is an aggressive cancer with increasing incidence (13, 14), which is most likely to develop in immunocompromised and elderly populations upon prolonged UV exposure (15, 16). About 80% of MCC are positive for MCPyV DNA integrated into the host genome (12). As for most PyV, MCPyV infections are widespread and predominantly asymptomatic. In fact, MCPyV is continuously shed from healthy skin with a prevalence of 60-80% (17-19). However, MCPyV DNA has also been isolated from respiratory, urine and blood samples (20), and the range of tissues in which persistent infection can be established is thus still unclear. The presence of integrated MCPyV DNA in MCC cells is thought to cause cancer through the

105 continuous expression of the transforming large T (LT) and small T (sT) antigens.
106 Integration of the viral DNA into the host cell genome is coupled to truncation of the
107 LT C-terminal domain, which is important for viral genome replication and can induce
108 p53 activity, triggering cell cycle arrest (21, 22). The viability of MCC cells depends
109 on expression of LT and/or sT, as pan-T knock-down in MCC-derived cells lead to
110 cell death (23, 24). Importantly, the cellular origin of MCC is still under debate. A
111 recent report suggests dermal fibroblasts as target cells for productive infection,
112 whereas Merkel cells are not permissive for virus entry or productive infection (25,
113 26). Thus, it remains unclear exactly which events give rise to MCC.
114
115 Since cell culture systems to produce sufficient quantities of infectious MCPyV are
116 not readily available, MCPyV vectors, so called pseudoviruses (PsV), are important
117 tools to study entry. As MCPyV does not contain detectable levels of VP3 (27), PsV
118 consist of VP1/VP2-only capsids that harbor a reporter plasmid (e.g. coding for
119 EGFP or luciferase). Expression of the reporter allows easy readout for successful
120 entry, i.e. delivery of the viral DNA to the site of transcription and replication (28). In
121 an effort to identify MCPyV-permissive cell lines and to better understand the tissue
122 tropism of MCPyV, the tumor cell library NCI-60 was screened for transducibility and
123 ability to support virus replication with MCPyV PsV and native virions, respectively
124 (29). Of those, A549 cells, a non-small cell lung cancer cell line, showed robust
125 transducibility with MCPyV PsV (28).
126
127 Since MCPyV is an emerging virus, little is known about the basic biology of the
128 virus, in particular how initial infection occurs. Initial studies on the mechanism of
129 MCPyV infection addressed cell surface interactions and cellular tropism of MCPyV
130 (25, 28, 30). MCPyV relies on binding sulfated glycosaminoglycans (GAGs) for initial

attachment similar to papillomaviruses (28). However, it also requires interaction with carbohydrates containing a linear sialic acid motif, i.e. Neu5Ac□2-3Gal, like other PyV (28, 30, 31).

Different viruses utilize distinct preexisting cellular endocytosis pathways for infectious entry (32). These endocytic pathways are characterized by a specific set of cellular factors and regulators facilitating endocytic vesicle formation. This set of cellular factors is used to distinguish different pathways. Well-studied endocytic pathways include clathrin-mediated endocytosis (CME), caveolar/lipid raft-mediated endocytosis, and macropinocytosis (33), which are essential for receptor-mediated endocytosis, turnover of plasma membrane receptors and fluid-phase uptake. To facilitate safe delivery and release of the viral genome to and at the site of replication, viruses are routed through specific intracellular target organelles, such as endosomes, the Golgi apparatus, or the endoplasmic reticulum (ER).

Host cell entry of most PyV occurs by caveolar/lipid raft-mediated endocytosis (34-37), whereas JC virus, for example, uses CME (38). After endocytosis, virions are routed through the endosomal pathway to be delivered to the ER (39). There, a chaperone- and disulfide isomerase-mediated uncoating step occurs, whereupon the modified particles are translocated into the cytosol by the ER-associated degradation machinery (40-43). In the current study, we aimed to identify the cellular requirements for virus entry into host cells to understand similarities and differences to other PyV. For this, we used small compound inhibitors of decisive cellular factors/processes during MCPyV infection. As functional controls, we employed well-studied viruses, including SV40, the papillomavirus HPV16, or the alphavirus Semliki Forest Virus (SFV) (36, 44, 45). In addition, we characterized the entry route of

MCPyV by ultrathin section transmission electron microscopy (TEM). Our results support a model in which MCPyV enters A549 cells by caveolar/lipid-raft dependent endocytosis, and where viruses are routed through the endosomal pathway to the ER. To our surprise, we found that MCPyV acquired a lipid membrane within endosomes. This membrane was absent once the virus located in the ER.

Results

MCPyV PsV cell binding and infection depend on sulfated glycosaminoglycans

To study the infectious entry requirements of MCPyV, we tested the susceptibility of the keratinocyte-derived cell lines HeLa and HaCaT in comparison to A549 cells. Using PsV we found that neither HeLa nor HaCaT cells showed GFP expression 72 h post infection and are thus poorly permissive for MCPyV entry (Fig. 1 A). We, therefore, decided to use A459 cells for our study, which allow for infectious internalization as previously described (29).

As initial strategy to elucidate the cellular route(s) of entry, perturbation of cellular processes followed by infection is key to identify factors/organelles facilitating MCPyV entry. The time course of MCPyV infectious entry into A549 cells was rather slow and plateaued after 72 h post infection (p.i.) (data not shown). Since indirect effects occur often after prolonged cellular perturbation, it is important to minimize such effects (46). For this, we compared siRNA-mediated knockdown, expression of dominant negative mutants, and small compound inhibition (data not shown). The efficacy and reliability of siRNA-mediated knockdown and expression of dominant mutants turned out to be questionable, as judged by infection of control viruses, so that we turned exclusively to small compound inhibition.

We first tested whether inhibition of acidification of endosomal compartments with the weak base ammonium chloride (NH_4Cl) perturbed MCPyV infection (47). In the presence of NH_4Cl, MCPyV infection was blocked in a dose-dependent fashion (Fig. 1 B) similar to infection with SV40 and HPV16, which served as positive controls (45,

48). This indicates the requirement for low pH in endosomal compartments during infectious internalization of MCPyV.

SV40 is directed to the ER for uncoating and subsequent translocation to the cytosol using ER resident disulfide oxidoreductases and the ER-associated degradation machinery (40). Dithiothreitol (DTT) is a powerful reducing agent and thus perturbs the cellular redox environment and disulfide oxidoreductase functions (49). Accordingly, DTT treatment arrests SV40 in the ER (40). We tested whether MCPyV was also sensitive to DTT treatment. MCPyV and SV40 infectivity was clearly reduced in the presence of DTT, whereas entry of Semiliki Forrest virus (SFV), which does not require a redox-driven ER uncoating step (44), was unaffected (Fig. 1 C).

Next, the ability of NH_4Cl or DTT to block MCPyV infection in relation to the time course of entry was tested. For this, the drugs were added different times p.i.. NH_4Cl and DTT exhibited a similar propensity to block MCPyV infection, where infectivity was inhibited upon early addition and increased with additions at later time point (Fig. 1 D). The increase at later time points indicates that the virus had passed the step blocked by the drugs. At 30 h p.i., about 50% of MCPyV had passed the acid-activated step, whereas the redox-dependent step appeared to occur slightly later (Fig. 1 D). The time courses indicate in addition a rather slow and asynchronous entry process akin to HPV16 (Fig. 1 D, (45)).

Prolonged treatment of cells with drugs that block endocytosis and trafficking can have indirect or cytotoxic effects. To address this problem, we employed an inhibitor swap approach in which cells were transiently treated with a drug of interest followed by replacement by another that blocks entry at a later stage, such as acid activation

in endosomes or redox-mediated uncoating in the ER (45, 46). Moreover, several different viruses served as positive and negative controls to assess the efficacy of treatment as well as the potential for pleiotropic drug effects.

Initially, as proof of feasibility, the requirement for sulfated GAGs was tested. MCPyV attachment to cells generally depends on such GAGs (28, 30, 31). Therefore, treatment with sodium chlorate ($NaClO_3$) was used to induce production of undersulfated GAGs (50). Treatment of A549 cells with 10, 20, or 30 mM $NaClO_3$ for 16 h prior to inoculation with MCPyV produced a dose-dependent reduction in infectivity (Fig. 1 E). HPV16 infectivity was similarly reduced, as expected (51). In contrast, infection with SV40 was unaffected, suggesting different requirements for the two PyV (Fig. 1 E). In addition, we tested the inhibitory effect of heparin, a highly sulfated GAG, on MCPyV infection. In line with previous results (28), preincubation of MCPyV pseudovirions with heparin efficiently blocked infection, only slightly less efficiently than the positive control HPV16 (Fig. 1 F). Influenza A virus (IAV) was used as a negative control, as IAV infection depends on interaction with sialic acids (52) and is independent of GAG binding. Heparin did not affect IAV infectivity (Fig. 1 F). Taken together, the results confirm that MCPyV infection requires interactions with sulfated cell-surface GAGs.

Inhibitory profile of MCPyV endocytosis

After confirming previous reports, we set out to characterize the endocytic pathway employed by MCPyV. First, CME was blocked with the small molecule inhibitor pitstop2, which interacts with the clathrin N-terminal domain and thereby interferes with assembly of the clathrin coat (53). Infection with MCPyV was unaffected by

239 treatment with pitstop2 (Fig. 2 A), similar to SV40, which enters cells by
240 caveolar/lipid-raft endocytosis (34, 36, 48). As expected, infection with SFV, which
241 enters cells by CME (44, 54), was efficiently reduced. Thus, MCPyV entry occurs
242 independently of CME.
243
244 Another important regulator of several endocytic pathways is dynamin-2 (Dyn2). The
245 large GTPase regulates scission of endocytic pits in several endocytic pathways, i.e.
246 CME, caveolae/lipid raft-mediated endocytosis, IL-2 endocytosis, and phagocytosis
247 (32). To study a potential Dyn2 involvement in MCPyV uptake, dynasore (an inhibitor
248 of the dynamin GTPase activity) was employed (55). SV40 served as a positive
249 control as it is known to depend on Dyn2 activity (56). Infection of MCPyV was
250 blocked dose-dependently by dynasore to a residual level of 22±13%, similar to
251 SV40 (Fig. 2 B). As a negative control, HPV16 was used. HPV16 enters host cells by
252 a clathrin-, caveolin-, cholesterol- and dynamin-independent, but actin-dependent
253 endocytic pathway (45). As expected, HPV16 infection remained unperturbed or
254 even increased after dynasore treatment (Fig. 2 B). This indicates that MCPyV is
255 endocytosed by a Dyn2-dependent pathway similar to SV40 but distinct from HPV16
256 endocytosis.
257
258 To further ascertain that MCPyV enters cells by a similar endocytic mechanism as
259 SV40, we perturbed cholesterol-dependent caveolar/lipid-raft endocytosis. To this
260 end, we treated cells with nystatin and progesterone, which sequester cholesterol
261 and prevent cholesterol synthesis, respectively (34, 56-59). As expected, infection
262 with MCPyV and SV40 were inhibited upon perturbation of cholesterol to residual
263 levels of 31±8% and 34±11%, respectively (Fig. 2 C), whereas HPV16 infection

264 remained unaffected as described previously (45). This suggests that MCPyV
265 infection, like SV40 infection, requires cholesterol-rich membrane domains (34).
266
267 Next, a potential role for macropinocytosis was assessed. The Na^+/H^+-exchanger
268 regulates macropinocytosis by controlling submembraneous pH, which in turn
269 regulates the formation of membrane protrusions (60). Ethylisopropylamiloride
270 (EIPA)-mediated inhibition of the Na^+/H^+-exchanger (61) is a classical treatment to
271 interfere with macropinocytosis. This treatment neither affected MCPyV nor SV40
272 infection (Fig. 2 D), whereas HPV16 infection was efficiently blocked as expected
273 (45). Thus, MCPyV endocytosis occurs independently of the Na^+/H^+-exchanger and,
274 consequently, also of macropinocytosis or related pathways.
275
276 In summary, MCPyV entry required cholesterol-rich membranes and dynamin, but
277 did not require clathrin or macropinocytic pathways. These observations are most
278 consistent with an entry pathway that employs caveolar/lipid-raft mediated
279 endocytosis.
280
281 **Regulation of MCPyV endocytosis depends on actin dynamics, Rho-like**
282 **GTPases and signaling via Tyr kinases and phosphatases PP1 and PP2A/B**
283
284 Next, we addressed functional regulators involved in endocytic processes with
285 respect to their role in MCPyV entry.
286
287 Actin polymerization is required for most endocytic pathways employed by viruses,
288 where formation of protrusions, intracellular transport or vesicle scission is facilitated
289 (32, 45). Cytochalasin D and jasplakinolide inhibit actin dynamics by either blocking

polymerization or depolymerization, respectively (62, 63). Both cytochalasin D and jasplakinolide efficiently blocked MCPyV and SV40 infection (Fig. 3 A, B), where the inhibitory effect of jasplakinolide was less pronounced for SV40. In contrast, CME-mediated uptake of SFV was unaffected by stabilization of actin filaments (Fig. 3 B) and increased upon actin depolymerization (Fig. 3 A).

Actin polymerization is most often regulated by the activity of pathway-specific Rho-like GTPases (32, 64, 65). Toxin B from *C. difficile* is a broad inhibitor of all Rho-like GTPases (66) and was hence used to assess the relevance of Rho GTPases for infection by MCPyV and SV40. As a negative control, we used HPV16 infection, which was not perturbed by treatment with toxin B, as expected (Fig. 3 C, (45)). Toxin B reduced MCPyV and SV40 infection to 15±18% and to 0.1±0.1% residual infection, respectively (Fig. 3 C). From this we conclude that Rho-like GTPases likely mediate actin-dependent steps during MCPyV endocytosis (Fig. 3 C). Analogous to SV40, the key step may be actin-dependent closure and fission of endocytic vesicles from the plasma membrane (56).

Ligand-induced activation of tyrosine kinases (tyr-kinases) regulates the activation of several endocytic pathways such as macropinocytosis and caveolar/lipid raft-mediated endocytosis, whereas CME and other pathways are tyr-kinase independent (32, 65). Genistein, a broad and efficient inhibitor of tyr-kinases (67), was used during infection with MCPyV, SV40, and HPV16. As expected for HPV16 and SV40, infection was blocked upon treatment with 200 µM genistein (Fig. 3 D). Interestingly, MCPyV infection was already sensitive to 50 µM genistein treatment (Fig. 3 D) suggesting a strong requirement for tyr-kinases, potentially at multiple levels.

316 Next, cellular phosphatases were inhibited with the broadly active sodium
317 orthovanadate, a competitive inhibitor of all phosphatases (68, 69). Entry of MCPyV,
318 SV40 and HPV16 were all strongly inhibited in the presence of orthovanadate (Fig. 3
319 E). Okadaic acid, a more specific inhibitor of phosphatases families PP1, PP2A and
320 PP2B (70), also inhibited MCPyV, SV40 and HPV16 (Fig. 3 F).
321
322 In summary, MCPyV entry is likely facilitated by dynamic actin rearrangement that is
323 regulated by Rho-like GTPases, as well as by the activity of tyr-kinases and PP1
324 and/or PP2A/B phosphatases.
325
326 **Intracellular trafficking of MCPyV requires endosomal acidification, functional**
327 **microtubular dynamics, and an intact redox environment**
328
329 Treatment with NH_4Cl reduced MCPyV infection indicating an acid-activation step
330 (Fig. 1 B). To test whether this acid-activated step occurred in endosomes,
331 bafilomycin A1, an inhibitor of the endosomal proton pump V-ATPase, was used (71).
332 Bafilomycin A1, like NH_4Cl, inhibited the infectivity of MCPyV, SV40, and HPV16 in a
333 dose-dependent fashion (Fig. 4 A). Thus, MCPyV depends on low endosomal pH for
334 either acid activation or trafficking within maturing endosomes.
335
336 Most intracellular transport occurs along microtubules (72). To assess microtubule
337 involvement in MCPyV infection, depolymerization of microtubules by treatment with
338 the polymerization blocker nocodazole was used (73). As reported previously, SV40
339 and HPV16 entry require the integrity of microtubules (Fig. 4 B). Similarly, MCPyV
340 infection strongly depended on intact microtubular dynamics (Fig. 4 B). This suggests

that MCPyV requires microtubules for transport of vesicular compartments or of the virus itself during host cell entry.

To study the involvement of intracellular transport processes from the ER to the Golgi apparatus in MCPyV entry, we used brefeldin A, which eventually leads to Golgi collapse into the ER (74). Upon perturbation with brefeldin A, infection with MCPyV, SV40, and HPV16 were blocked (Fig. 4 C). This indicates that infection with these viruses requires the functional integrity of the secretory ER/Golgi compartments.

Another hint for an involvement of the ER during infectious internalization can be drawn from the perturbation of the cellular redox environment by DTT. At the concentrations used, DTT interferes mostly with the formation of disulfide bonds during folding in the ER but not with existing disulfide bonds in folded proteins (49). Since MCPyV infection was blocked by DTT (Fig. 1 C), it is reasonable to assume that MCPyV like SV40 requires an ER step for host cell entry, possibly for uncoating and translocation into the cytosol.

After escape from the ER, SV40 is thought to be imported into the nucleus via the nuclear pore complexes (75). In contrast, HPV16 requires cell cycle progression, i.e. nuclear envelope breakdown, for nuclear entry (76, 77). To address whether MCPyV infection depends on mitotic activity for nuclear entry, we blocked cells in S-phase using aphidicolin, an inhibitor of DNA polymerase alpha and delta (78). MCPyV entry was efficiently blocked by aphidicolin to a similar extent as HPV16 (Fig. 4 D). The RNA virus SFV replicates in the cytoplasm and therefore served as a negative control (79). SFV infection was not affected by aphidicolin treatment (Fig. 4 D), as

366 expected. These results indicate that MCPyV infection may depend on the mitotic
367 activity of the host cells.
368
369 **MCPyV is internalized into small, non-coated vesicles**
370
371 Our inhibition studies indicate that MCPyV and SV40 use similar pathways to infect
372 cells. To confirm this notion, we examined virion trafficking using TEM. Localization
373 of virus particles was assessed 2, 8, 16, 24 and 48 h p.i.. Interestingly, the virus
374 localized to several specific cellular compartments at each time-point, in line with
375 asynchronous internalization and trafficking of the MCPyV particles. Virus particles
376 were readily detectable bound to the cell surface (Fig. 5 A). In addition, they were
377 found within small, inward budding membrane invagination without any visible protein
378 coat (Fig. 5 A, B). Interestingly, virions resided in two distinct but equally frequent
379 populations of invaginations. In one class of invagination, the plasma membrane
380 appeared to make close contact with the virion surface, while the second class of
381 invagination exhibited 10 nm ± 8 nm distances between the membrane and the virion
382 surface. The first class of invagination is reminiscent of prior observations for SV40,
383 which is known to make close contact with the sialylated headgroups of plasma
384 membrane glycolipids (80, 81). The latter class of invagination suggests possible
385 interactions between the virion and a glycoprotein receptor with a large ectodomain,
386 such as an HSPG. In addition, MCPyV virions were found within intracellular vesicles
387 without an apparent protein coat (Fig. 5 C). These data, and the absence of virus in
388 large, coated or tubular invaginations, is consistent with MCPyV uptake by
389 caveolar/lipid raft-mediated endocytosis rather than uptake by macropinocytosis,
390 CME or glycosphingolipid-enriched carriers (58, 81-83).
391

392 **MCPyV traffics via the endolysosomal route to the ER**

393

394 After initial uptake into endocytic vesicles, MCPyV particles were found in early
395 endosomal compartments and later accumulated in late endosomal/lysosomal
396 structures (Fig. 6 A, B). Other polyomaviruses, such as SV40, JCPyV and BKPyV,
397 are then trafficked to the ER via Golgi- and non-Golgi routes. In the ER,
398 oxidoreductases and chaperones mediate partial disassembly of the virions
399 (uncoating) and transfer of partially disassembled virions into the cytosol (40, 81, 84-
400 86). MCPyV was undetectable in the Golgi apparatus (Fig. 6 D), the cytosol, or the
401 nucleus. Similar to other PyV, MCPyV was observed in the lumen of the ER, but only
402 to a minor extent (Fig. 6 C).

403

404 Taken together, the EM results thus support the conclusion that MCPyV and SV40
405 use similar infectious entry pathways.

406

407 **MCPyV acquires a lipid envelope in endosomal compartments**

408

409 In addition to the observations described above, we surprisingly found MCPyV
410 particles with what appeared to be a double layer lipid membrane in endosomal
411 compartments (Fig. 7 A, B). The membrane tightly enveloped the particles. The
412 enveloped virions were easily detectable in maturing and late endosomes as well as
413 endolysosomes similar to non-enveloped particles. In fact, both enveloped and non-
414 enveloped particles were detectable side by side in the same endosomes (Fig. 7 C,
415 enveloped black arrows vs. non-enveloped white arrow). This suggested that the
416 process of acquiring a lipid envelope occurs during viral passage of the endosomal
417 pathway rather than in distinct, specialized organelles. It is unclear whether the

418 enveloped particles are part of the productive infectious entry pathway or are instead
419 a dead end for the virus. Possibly, this phenotype reflects a new mode of antiviral
420 defense or a mechanism to evade endosomal degradation.
421
422 **The role of sialic acid for MCPyV entry**
423
424 Previous studies showed that mutations in the sialic acid binding pocket of MCPyV
425 VP1 rendered the particle non-infectious but did not perturb binding to cells (30).
426 Hence, sialic acid interaction is essential for infectious entry, whereas initial
427 attachment occurs mainly by GAG engagement. Since we observed MCPyV particles
428 in endocytic pits in two distinct populations that may reflect binding to gangliosides
429 and HSPGs, two sialic acid binding site mutants (W76A and Y81V) were followed
430 using EM. The mutant PsV assembled without visible defects (Fig. 8 A, B i, C i), but
431 were unable to mediate infection in A549 cells (Fig. 8 D), as expected (30). To verify
432 the desired glycan binding abilities of the sialic acid mutants, we conducted
433 saturation transfer difference (STD-) NMR experiments to probe for binding of
434 sialylated oligosaccharides and GAG oligosaccharides to MCPyV wild-type and
435 mutant virus-like particles (VLPs). STD-NMR makes use of energy transfer from
436 proteins to their ligands upon binding and thus allows determination of binding
437 specificities by comparing the changes in the resonance frequencies of the ligand
438 molecules in association with wild-type or mutant viruses (30, 87). Here,
439 3'sialyllactose (3'SL) and a chemically well-defined heparan sulfate (HS)-
440 pentasaccharide, Arixtra (Ax), were chosen as a minimal sialylated MCPyV ligand
441 and a short GAG oligosaccharide, respectively (Fig. 9 A, B). STD-NMR showed that
442 the GAG pentasaccharide bound to wild-type VLPs as well as to the W76A mutant
443 (Fig. 9 B ii vs. iii). In contrast, 3'SL bound both wild-type and Y81V mutant VLPs but

no saturation transfer was observed from the W76A mutant to 3'SL (Fig. 9 A ii vs. iii vs. iv). Consistent with previous crystallographic and NMR-based results (30), only resonances from the 3'SL sialic acid and galactose rings were observed. For the HS pentasaccharide (Fig. 9 B), on the other hand, magnetization transfer was observed almost equally for all five monosaccharide units, with the non-sulfated GlcA ring being the only unit, whose resonances were somewhat underrepresented in the STD-NMR spectra in comparison to the ^{1}H reference spectrum of the free pentasaccharide. This suggests that the GlcA ring is the least important determinant in the interaction. In summary, these results confirm that the W76A mutant is defective in sialic acid binding, whereas Y81V remained partially able to interact with the 3'SL ligand under these conditions. Furthermore, the binding site for GAGs apparently remained intact upon mutation suggesting that the GAG binding site is spatially distinct from the sialic acid interaction site.

EM analyses showed that the W76A and Y81V mutants readily bound to the A549 cells, presumably through interactions with HSPGs (Fig. 8 B ii, C ii; (30)). Interestingly, both mutants were exclusively observed in the second class of invaginations (i.e., invaginations with a >5 nm gap between the plasma membrane and the virion surface (Fig. 8 B ii, C ii). This observation supports the concept that the first class of invaginations are formed through short range contacts between the virion and sialylated glycolipids (which the mutants fail to bind), while the second class of invagination involves interactions with bulkier HSPGs.

Discussion

MCPyV is the first human PyV clearly linked to the development of a specific cancer (12). Initial studies on the principal mechanism of infection confirmed the requirement of sulfated glycosaminoglycans for attachment and sialylated glycans for infectious uptake into host cells, which may, in fact, reflect a common mechanism for several PyV (28, 30, 31, 88). To extend our knowledge of the mechanism of initial infection, we addressed additional cellular requirements and routes of virus entry. Our evidence from inhibitor and morphological studies indicates that MCPyV infects cells asynchronously via a caveolar/lipid-raft dependent endocytic pathway that is similar to that used by SV40. After internalization, virus particles were routed to endolysosomal compartments and the ER. Our preliminary evidence suggests that entry of MCPyV depends on progression of the cell cycle, potentially for the nuclear entry step.

The initial step of virus entry is binding to target cells. Previous work suggested that the interaction with sulfated GAGs is required for MCPyV binding, whereas sialic acids have a post attachment role (28). We confirmed that heparin, a highly sulfated GAG, was able to compete for cell surface GAGs thus prohibiting binding and infection of A549 cells. In addition, we addressed the role of GAGs and sialic acids concerning their influence on endocytic uptake. Interestingly, we observed two populations of MCPyV particles on the plasma membrane and in endocytic pits differing in their distance to the limiting membrane, possibly representing the different binding receptor species. In principle, these could reflect binding to proteinaceous receptors with a large ectodomain (wide pits) or gangliosides (sialylated lipids, tight pits), as shown for JC virus uptake via sialylated glycoproteins (89) and SV40 uptake

by ganglioside interaction (90). Alternatively, the proteinaceous receptor may constitute HSPGs.

To further unravel the individual roles of sialylated glycans and GAGs during MCPyV entry, two sialic acid binding site mutants (W76A and Y81V, (30)) were subjected to a STD-NMR-based binding assay. These studies confirmed that binding to sialylated glycans was abolished for W76A, but not for Y81V, whereas either mutant retained binding of the HS pentasaccharide. This finding indicates that the binding sites for sialic acid and sulfated GAGs do not overlap and are independent of each other. The most striking difference between wild-type MCPyV and the sialic acid binding site mutants in the TEM experiments was that the mutants were exclusively detected in endocytic pits with the large distances between viral particles and plasma membrane layers. The most likely interpretation of these observations is thus that the large distance reflects binding to a proteinaceous receptor containing sulfated GAGs such as HSPGs, whereas tightly fitted binding to the plasma membrane reflects ganglioside engagement. Since uptake of HSPGs has been suggested to occur primarily through flotillin- and dynamin-dependent endocytosis (91, 92), MCPyV internalization in wider pits via HSPGs seems distinct from the caveolar/lipid raft-mediated internalization required for infection. It thus appears that MCPyV internalization via HSPGs is a dead end. While W76A and Y81V MCPyV were readily observable in endosomes, they were not detected in the ER. Hence, the W76A and Y81V mutations likely rendered the particles non-infectious, as they were unable to engage sialic acid containing gangliosides efficiently and thus were not taken up by an infectious pathway that routes the virus to ER.

Since the sialic acid binding mutants were found in endosomes but not the ER, the interaction with sialic acid receptors is crucial for routing the virus to the ER. This is in line with previous work indicating that branched sialylated glycosphingolipids targets murine polyomavirus (mPyV) and SV40 from endolysosomes to the ER (36, 48, 80, 93). The role of HSPGs remains less clear. It may be that MCPyV interacts with sulfated GAGs simply, because they may serve as an initial high affinity attachment factor, which facilitates later interaction with low affinity glycosphingolipids. An alternative mechanism may be the induction of a conformational change in the virus capsid upon GAG binding that may facilitate uncoating and transfer to the secondary receptor, as it has been described for HPV16, a virus with a similar tissue tropism (51, 94). However, such GAG-induced conformational changes have no precedent among other PyVs. Of note, JC PyV can utilize two distinct pathways for infectious internalization, where one depends on interaction with sulfated GAGs and the other relies on sialic acid binding, this effect could depend on the host cell type (88). As the niche(s) for MCPyV infection remain only partially understood, the role of HSPGs in MCPyV entry may thus depend on specific cell types that are being infected *in vivo.*

Receptor engagement leads to the endocytosis of MCPyV. In line with our initial hypothesis that infectious entry of MCPyV may follow a path similar to that of SV40, our inhibitory experiments showed that infectious entry was independent of clathrin and the activity Na^+/H^+-exchanger but required dynamin and cholesterol, as well as actin dynamics. Since MCPyV particles were not found in coated pits or membrane protrusions, entry does not involve CME or macropinocytosis. The combined requirements for dynamins, cholesterol and actin dynamics indicated endocytosis by caveolar/lipid raft mediated endocytosis. Dynamins are also involved in phagocytosis and endocytosis of interleukin-2 (IL-2), both of which also require actin and lipid

rafts/cholesterol (32). Phagocytosis occurs only in specialized cells and it is characterized by long outward protrusions that close around large cargos (95). Thus, an involvement of phagocytosis can be excluded similar to macropinocytosis. IL-2 endocytosis, on the other hand, occurs into small, inward budding vesicles, which are mostly formed at the base of an outward protrusion (96). Such initial pits containing MCPyV can be found in the electron micrographs, however in the majority of cases, MCPyV is taken up into small vesicle from flat membrane regions, which makes IL-2-like endocytosis seem unlikely.

Caveolar/lipid raft-mediated endocytosis routes cargos into endosomal compartments (48, 97). We found MCPyV particles in high abundance in endosomal compartments resembling endosomes, lysosomes, multivesicular and lamellar bodies. We also observed small numbers of MCPyV virions in the ER. Retrograde trafficking from endosomes to the ER is a general mechanism employed by PyVs. The low frequency of ER-localized MCPyV virions is similar to prior observations of mPyV entry (93) and hints at a bottleneck for trafficking from endosomes to the ER. Murine PyV as well as JC and BK PyV have been shown to require acidic pH environments in the endolysosomal compartment presumably for a conformational change facilitating membrane penetration after translocation into the ER by a yet unknown mechanism (86, 98, 99). For MCPyV, acidification in the endolysosomal system may serve a similar role.

MCPyV infection is sensitive to DTT treatment (Fig. 1 C) and may therefore be dependent on the redox environment within the ER. In analogy to SV40, uncoating and membrane translocation to the cytoplasm may occur in the ER with the help of the ERAD machinery and cytoplasmic chaperones (39, 40).

As a final step, the viral genome must be delivered to the nucleus, which is the site of early gene expression and replication for PyV. Interestingly, we found that MCPyV infection was sensitive to cell cycle block in S-phase, which indicates that mitosis is required for completion of MCPyV entry. Previous work on HPV16 identified its dependence on mitotic activity of the target cells, which allows delivery of the viral genome to the nucleus upon nuclear envelope breakdown (77, 100). However, SV40 has been described to enter the nucleus of interphase cells through the nuclear pore complex by making use of nuclear localisation signals in the viral capsid proteins after ERAD-dependent partial disassembly (40, 101-103). It remains thus unclear, why MCPyV target cells actively progressing through the cell cycle. Nevertheless, our findings are in line with the importance of WNT signalling during infection of dermal fibroblasts (25).

To our surprise, we regularly observed enveloped particles in endosomal compartments. It remains unclear when and how these virions acquire a membraneous envelope, whether this reflects an antiviral mechanism or whether it is part of the infectious entry mechanisms. It is conceivable that MCPyV uses the ESCRT machinery that generates intraluminal vesicles (ILVs) in multivesicular bodies (104). Alternatively, it may wrap itself in a membrane within the late endosomal/lysosomal compartment. The membrane could theoretically shield the virus from hydrolases, and may give it the time to persist until infection can be completed e.g. by progression through the cell cycle. Alternatively, these enveloped virus particles might arise through an unknown antiviral mechanism. Future studies will address the relevance of such enveloped particles for the infectious route.

599 In the light of our experiments and previous reports (28, 30), we propose that MCPyV
600 attachment and internalization, at least in the model A549 cell line, is mediated by
601 HS-type GAGs but that additional sialic acid binding is essential to route the
602 internalized virus to the productive infection pathway of retrograde ER trafficking.
603 However, entry into the ER seems to be a bottleneck for infections.
604
605

606 **Materials and Methods**

607 **Cell lines, antibodies, and reagents**

608 HeLa cells were from ATCC. A549 cells were a kind gift from C. Buck (NIH, National
609 Cancer Institute, Bethesda, MD, USA). CV1 cells were a kind gift from J. Kartenbeck
610 (DKFZ, Heidelberg, Germany). BHK Helsinki cells were a kind gift from A. Helenius
611 (ETH Zürich, Switzerland)**.** 293TT cells were a kind gift from J. Schiller (NIH, National
612 Cancer Institute, Bethesda, MD, USA). Aphidicolin, EIPA, cytochalasin D,
613 nocodazole, nystatin, NH_4Cl, $NaClO_3$, heparin, and sodium orthovanadate were from
614 Sigma-Aldrich. Bafilomycin A1, genistein, progesterone were from Applichem.
615 Brefeldin A, cyclosporine A, jasplakinolide, okadaic acid were from Calbiochem.
616 Dynasore was from Merck. Pitstop2 was from Abcam. RedDot2 was from VWR.
617
618 **Viruses**
619 MCPyV pseudoviruses (PsV) containing a GFP reporter plasmid (MCPyV-GFP) were
620 produced by transfection of 293TT cells with pwM2m, ph2m and phGluc as described
621 previously (105, 106). In brief, 293TT cells were transfected with the indicated
622 plasmids. After 48 h, cells were harvested and lysed. For optimal maturation, lysates
623 were incubated for further 24 h with 25 mM ammonium sulfate (pH 9.0) (107).
624 MCPyV PsVs were purified on a 25%-39% linear OptiPrep gradient (Sigma-Aldrich).
625 HPV16 pseudoviruses containing a GFP reporter plasmid (HPV16-GFP) were
626 produced by transfection of 293TT cells with p16SheLL and pCIneo as described
627 previously (105, 106). The procedure was similar to MCPyV production above.
628 SV40 and SFV were produced as described previously (40, 108).
629
630 **Infection assays upon inhibitor treatment**

631 Infection assays with MCPyV, HPV16, and SV40 were conducted in 96well plates,
632 where 3000 or 10000 A549 cells were seeded in RPMI (5% FCS and 2 mM
633 glutamine) at least 6 h prior to infection. Cells were treated with 80 µL of the following
634 inhibitors at the indicated concentrations diluted in RPMI (5% FCS, 2 mM glutamine)
635 or SV40 infection medium (RPMI with 3% BSA, 10 mM HEPES, pH 6.8): overnight
636 preincubation - nystatin/progesterone, sodium chlorate, and toxin B; 30 min
637 preincubation – bafilomycin A1, brefeldin A, cytochalasin D, dithiotreitol, dynasore,
638 EIPA, genistein, jasplakinolide, NH_4Cl, nocodazole, okadaic acid, pitstop2, sodium
639 orthovanadate, wortmannin. Virus was diluted in RPMI (5% FCS, 2 mM glutamine) or
640 SV40 infection medium and 20 µL of the inoculum were added to each well. MCPyV
641 samples were incubated for 30 h until the inhibitor dilutions were exchanged to RPMI
642 containing 10 mM NH_4Cl and 10 mM HEPES, pH 7.4 and incubated for further 42 h.
643 Samples were fixed by addition of a final 4% paraformaldehyde (PFA) to the wells.
644 Nuclei were stained with RedDot2. Infection scored by analysis of GFP expression by
645 microscopy (Zeiss Axio Observer Z1 equipped with a Yokogawa CSU22 spinning
646 disc module and a CoolSnap HQ camera; Visitron Systems GmbH). Infection with
647 HPV16 was similar to MCPyV but for the exchange of medium to DMEM containing
648 10 mM NH_4Cl and 10 mM HEPES, pH 7.4 occurred after 12 h post infection and
649 fixation was done after total 48 h. SV40 inoculum was replaced by fresh DMEM
650 containing 5 mM DTT after 10 h incubation until fixation after 24 h. Cells were
651 incubated with SFV for 4 h until fixation. Samples were fixed as above. For detection
652 of infection, SV40 and SFV samples were stained with an anti-LTag antibody (*sc-*
653 *20800*) or SFV glycoprotein antibody (110), respectively, and an AF488-coupled
654 secondary antibody; subsequently nuclei were stained with RedDot2. Infection was
655 scored by microscopy (Zeiss Axio Observer Z1 equipped with a Yokogawa CSU22
656 spinning disc module and a CoolSnap HQ camera; Visitron Systems GmbH). Cell

numbers and infection indices were determined by using the MatLab script Infection Counter as described before (40, 48).

Alternatively, the effects of single inhibitors on MCPyV and control virus infection were tested in a flow cytometry-based assay. Here, $3x10^4$ A549 cells were seeded in 24-well plates or $5x10^4$ HeLa cells in 12-well plates or $2.5x10^5$ BHK Helsinki cells in 12-well plates 6-8 h prior to treatment with aphidicolin over night. The compound was renewed before cells were infected with MCPyV, HPV or SFV, respectively. Aphidicolin was renewed daily until fixation of the cell at 72 h p.i. by trypsinization and subsequent addition of 4% paraformaldehyde. The percentage of GFP-positive cells was measured by flow cytometry using a BD FACScalibur.

Electron microscopy

For negative staining EM of virus particles, about $8x10^6$ PsV in PBS/0.8M NaCl were absorbed for 5 min on formvar coated, carbon sputtered grids. Particles were contrasted for 7 min with 1% phosphotungstic acid. Samples were analyzed directly after drying. The sample was analyzed at 80 kV on a FEI-Tecnai 12 electron microscope (FEI, Eindhoven, Netherlands). Images of selected areas were documented with Olympus Veleta 4k CCD camera.

For ultrathin sectioning transmission EM, virus particles were added for 2 h, 8 h and 16 h to A549 cells before fixation with 2.5% glutaraldehyde in PBS. Samples were post-fixed with 0.5% OsO_4, block stained with 0.5% uranyl acetate and after dehydration embedded in Epoxyresin. 60nm ultrathin sections were cut and counterstained with uranyl acetat and lead. Images of selected areas were documented with Olympus Veleta 4k CCD camera.

NMR spectroscopy

683 NMR experiments were conducted at 283 K using a 600 MHz Bruker Avance
684 spectrometer equipped with a TXI triple resonance room temperature probe head. 3
685 mm I.D. NMR tubes with 200 µL sample volume were used. Each sample contained
686 55.6 nM MCPyV VLPs (i.e. 20 µM of the major capsid protein VP1) - either wild-type
687 or mutant - and 1 mM oligosaccharide (either 3'SL or the Arixtra GAG-
688 pentasaccharide). Prior to NMR sample preparation, VLPs were dialysed in Slide-A-
689 Lyzer MINI dialysis devices (Thermo Fisher Scientific) against 150 mM NaCl, 1 mM
690 $CaCl_2$, pH 6.0 in D_2O. 3'SL (Carbosynth) was added from a 40 mM stock solution
691 prepared in pure D_2O and Arixtra was added from a 7.2 mM stock solution in 150 mM
692 NaCl, 1 mM $CaCl_2$, pH 6.0 in D_2O, dialysed from ready-to-inject syringes (Aspen).
693 For 3'SL-containing samples, off- and on-resonance frequencies in STD-NMR
694 experiments were set to −30 ppm and 7.3 ppm, respectively, while -30 ppm and -0.5
695 ppm were used for Arixtra-containing samples, owing to the different chemical shift
696 ranges of both glycans. The irradiation power of the selective pulses was set to 57
697 Hz. The saturation time was 2 s and a total relaxation delay of 3 s was used. A 50-ms
698 continuous-wave spin-lock pulse with a strength of 3.2 kHz was employed to
699 suppress residual protein signals. A total number of 512 scans and a total number of
700 10,000 points were collected and spectra were multiplied with a Gaussian window
701 function prior to Fourier transformation.
702
703 **MCPyV VLP preparation for NMR spectroscopy**
704 MCPyV VLPs were produced essentially according to a published protocol (111). The
705 pwM and ph2m vectors coding for MCPyV VP1 and VP2, respectively, ((27), see also
706 www.addgene.org) were used at a 5:1 ratio for transfection of 293 TT cells. OptiPrep
707 was omitted during the purification and replaced with two CsCl density gradient
708 centrifugation steps.

Acknowledgements

We would like to thank N. Cordes and E. Weghake (Cellular Virology, Münster, Germany) for technical support during virus production and infection experiments. Thanks also to members of the Schelhaas laboratory for helpful comments on this manuscript. This work was supported by funding to MS by the German Research Foundation (DFG EXC 1003 (partly)) and within the InfectERA initiative by funding from the Federal Ministry for Education and Research (BMBF, 031L0095A). Further support from the DFG to BSB is also acknowledged (1294/3-1 belonging to FOR2328 'Virocarb').

Figure legends

Figure 1: MCPyV infection is slow and asynchronous, and relies on interaction with sulfated glycans. (A) A549, HeLa or HaCaT cells were infected with increasing amounts of MCPyV PsV. Depicted are relative infection values (%) related to the MCPyV amount yielding 20% absolute infection in A549 cells ± SD (1x = 80 ng VP1). (B) A549, CV-1 or HeLa cells were infected with MCPyV, SV40 or HPV16, respectively, in the presence of indicated concentrations of NH_4Cl. (C) A549, CV-1 or BHK cells were infected with MCPyV, SV40 or SFV, respectively, in the presence of indicated concentrations of DTT. (D) A549 cells were infected with MCPyV for total 72 h, while 10 mM NH_4Cl or 5 mM DTT was added at indicated h p.i.. (E) A549, CV-1 or HeLa cells were infected with MCPyV, SV40 or HPV16, respectively, upon pretreatment with indicated concentrations of $NaClO_3$ for 16 h prior to infection. (F) A549 were infected with MCPyV or IAV, and HeLa cells were infected with HPV16 virions, which were treated with indicated concentrations of heparin for 1 h prior to

735 infection. (B-F) Depicted are averages of relative infection values to untreated
736 controls ± SD from at least 3 independent experiments.
737
738 **Figure 2: MCPyV infection is dynamin- and cholesterol-dependent, but**
739 **independent from clathrin and Na^+/H^+-exchangers.** (A) A549, CV-1 or BHK cells
740 were infected with MCPyV, SV40 or SFV, respectively, in the presence of indicated
741 concentrations of pitstop2. (B-D) A549, CV-1 or HeLa cells were infected with
742 MCPyV, SV40 or HPV16, respectively, in the presence of indicated concentrations of
743 dynasore (B), nystatin/progesterone (C), and EIPA (D). Depicted are percentages of
744 infection values relative to solvent treated controls ± SD of at least 3 independent
745 experiments.
746
747 **Figure 3: MCPyV infection is dependent on actin, RhoGTPases, tyr-kinases,**
748 **and cellular phosphatases.** (A-B) A549, CV-1 or BHK cells were infected with
749 MCPyV, SV40 or SFV, respectively, in the presence of indicated concentrations of
750 cytochalasin D (A) or jasplakinolide (B). (C-F) A549, CV-1 or HeLa cells were
751 infected with MCPyV, SV40 or HPV16, respectively, in the presence of indicated
752 concentrations of toxin B (C), genistein (D), sodium orthovanadate (E), or okadaic
753 acid (F). Depicted are percentages of infection values relative to solvent treated
754 controls ± SD of at least 3 independent experiments.
755
756 **Figure 4: MCPyV infection requires endosomal acidification, functional**
757 **microtubular dynamics, and an intact redox environment.** (A-C) A549, CV-1 or
758 HeLa cells were infected with MCPyV, SV40 or HPV16, respectively, in the presence
759 of indicated concentrations of bafilomycin A (A), nocodazol (B), and brefeldin A (C).
760 A549, BHK, or HeLa cells were infected with MCPyV, SFV or HPV16 respectively, in

761 the presence of indicated concentrations of aphidicolin (D). Depicted are percentages
762 of infection values relative to solvent treated controls ± SD of at least 3 independent
763 experiments.
764
765 **Figure 5: MCPyV is taken up into tight-fitting inward budding pits.** (A-C) A549
766 cells were infected with MCPyV particles for 2-24 h before fixation with
767 glutaraldehyde. Cells were processed for TEM according to standard procedures.
768 Images of early entry events were taken. Scale bar 100 nm.
769
770 **Figure 6: MCPyV travels through the endolysosomal system to the ER omitting**
771 **the Golgi.** (A-D) A549 cells were infected with MCPyV particles for 2-24 h before
772 fixation with glutaraldehyde. Cells were processed for TEM according to standard
773 procedures. Virus particles were found in endosomal compartments (A, B) and in the
774 ER (C). MCPyV was absent from the Golgi (D). Scale bar 100 nm.
775
776 **Figure 7: MCPyV virions acquire a membrane envelope during cell entry.** (A-C)
777 A549 cells were infected with wild-type MCPyV particles before fixation with
778 glutaraldehyde. Cells were processed for TEM according to standard procedures.
779 Images of virus particles in intracellular compartments were taken after 8 h and 16 h
780 p.i.. Note the envelope around the virus particles in the representative endosomal
781 compartments. C) Note that enveloped particles (black arrows) are found side-by-
782 side with non-enveloped virions (white arrow) in the same organelle. Scale bars 100
783 nm; Scale bar inset 50 nm.
784
785 **Figure 8: MCPyV sialic acid binding mutants are taken up into A549 cells but**
786 **fail to mediate infection.** (A-C i) MCPyV wild-type and mutant particles were

analyzed by electron microscopy after negative staining. Depicted are representative images of virions. Scale bars: 50 nm. (B-C ii and iii) A549 cells were infected with W76A and Y81V MCPyV particles for 2-24 h before fixation with glutaraldehyde. Cells were processed for TEM according to standard procedures. Images of virus particles in endocytic pits and in intracellular compartments were taken after 8 h (ii) and 16 h p.i. (iii), respectively. Scale bar 100 nm for ii and 200 nm for iii. (D) 60 ng (1x), 300 ng (5x) and 600 ng (10x) of MCPyV wild-type and W76A and Y81V mutant particles were used in an infection assay with A549 cells for 72 h.

Figure 9: MCPyV sialic acid binding mutants are capable of GAG binding. A) STD-NMR difference spectra of MCPyV VLPs with 3'sialyllactose (3'SL) and reference spectra. From top to bottom: i) VLP ^{1}H 1D reference spectrum; ii) STD-NMR spectrum of WT VLPs with 3'SL exhibiting saturation transfer from the capsid to 3'SL; iii) same spectrum for Y81V mutant VLPs; iv) same spectrum with W76A mutant VLPs showing no transfer to 3'SL; v) 3'SL ^{1}H 1D spectrum for comparison. Small molecule impurities are observed in the VLP preparation (i and iv), some of which are buffer components (sharp resonances with asterisks), others are unidentified molecules that are likely associated with the capsids (broad resonances with asterisks, the peak broadening suggests slow molecular tumbling, i.e. association with the VLPs). HDO signals were truncated for the sake of visibility. B) STD-NMR difference spectra of MCPyV VLPs with a GAG pentasaccharide (Arixtra, Ax) and reference spectra. From top to bottom: i) VLP ^{1}H 1D reference spectrum; ii) STD-NMR spectrum of WT VLPs with pentasaccharide exhibiting saturation transfer from the capsid to the GAG; iii) same spectrum with W76A mutant VLPs; iv) GAG ^{1}H 1D spectrum for comparison. Saturation transfer to the GAG is observed for the WT

and the W76A mutant that does not bind to 3'SL (Fig. 8 A iv). HDO signals were truncated for the sake of visibility.

References

1. **Gjoerup O, Chang Y.** 2010. Update on Human Polyomaviruses and Cancer. Advances in Cancer Research **106:**1-51.
2. **Moens U, Calvignac-Spencer S, Lauber C, Ramqvist T, Feltkamp MCW, Daugherty MD, Verschoor EJ, Ehlers B, Ictv Report C.** 2017. ICTV Virus Taxonomy Profile: Polyomaviridae. J Gen Virol **98:**1159-1160.
3. **Gross L.** 1953. A filterable agent, recovered from Ak leukemic extracts, causing salivary gland carcinomas in C3H mice. Proc Soc Exp Biol Med **83:**414-421.
4. **Eddy BE, Borman GS, Grubbs GE, Young RD.** 1962. Identification of the oncogenic substance in rhesus monkey kidney cell cultures as simian virus 40. Virology **17:**65-75.
5. **Chang Y, Moore PS.** 2012. Merkel cell carcinoma: a virus-induced human cancer. Annu Rev Pathol **7:**123-144.
6. **DeCaprio JA, Garcea RL.** 2013. A cornucopia of human polyomaviruses. Nat Rev Microbiol **11:**264-276.
7. **Gardner S, Field A, Coleman D, Hulme B.** 1971. New Human Papovavirus (B.K.) Isolated from Urine after Renal Transplantation. The Lancet **297:**1253-1257.
8. **Padgett B, Zurhein G, Walker D, Eckroade R, Dessel B.** 1971. Cultivation of Papova-Like Virus from Human Brain with Progressive Multifocal Leucoencephalopathy. The Lancet **297:**1257-1260.

9. **Kean JM, Rao S, Wang M, Garcea RL.** 2009. Seroepidemiology of human polyomaviruses. PLoS Pathog **5:**e1000363.

10. **Stolt A, Sasnauskas K, Koskela P, Lehtinen M, Dillner J.** 2003. Seroepidemiology of the human polyomaviruses. J Gen Virol **84:**1499-1504.

11. **Walker DL, Padgett BL.** 1983. The epidemiology of human polyomaviruses. Prog Clin Biol Res **105:**99-106.

12. **Feng H, Shuda M, Chang Y, Moore PS.** 2008. Clonal integration of a polyomavirus in human Merkel cell carcinoma. Science **319:**1096-1100.

13. **Hodgson NC.** 2005. Merkel cell carcinoma: Changing incidence trends. Journal of Surgical Oncology **89:**1-4.

14. **Lemos B, Nghiem P.** 2007. Merkel cell carcinoma: more deaths but still no pathway to blame. J Invest Dermatol **127:**2100-2103.

15. **Engels EA, Frisch M, Goedert JJ, Biggar RJ, Miller RW.** 2002. Merkel cell carcinoma and HIV infection. The Lancet **359:**497-498.

16. **Locke FL, Rollison DE, Sondak VK.** 2015. Merkel cell carcinoma and immunosuppression: what we still need to know. J Natl Cancer Inst **107**.

17. **Hampras SS, Michel A, Schmitt M, Waterboer T, Kranz L, Gheit T, Fisher K, Sondak VK, Messina J, Fenske N, Cherpelis B, Tommasino M, Pawlita M, Rollison DE.** 2015. Merkel cell polyomavirus (MCV) T-antigen seroreactivity, MCV DNA in eyebrow hairs, and squamous cell carcinoma. Infect Agent Cancer **10:**35.

18. **Schowalter RM, Pastrana DV, Pumphrey KA, Moyer AL, Buck CB.** 2010. Merkel cell polyomavirus and two previously unknown polyomaviruses are chronically shed from human skin. Cell Host Microbe **7:**509-515.

19. **Pastrana DV, Pumphrey KA, Cuburu N, Schowalter RM, Buck CB.** 2010. Characterization of monoclonal antibodies specific for the Merkel cell polyomavirus capsid. Virology **405:**20-25.

20. **Spurgeon ME, Lambert PF.** 2013. Merkel cell polyomavirus: a newly discovered human virus with oncogenic potential. Virology **435:**118-130.

21. **Shuda M, Feng H, Kwun HJ, Rosen ST, Gjoerup O, Moore PS, Chang Y.** 2008. T antigen mutations are a human tumor-specific signature for Merkel cell polyomavirus. Proc Natl Acad Sci U S A **105:**16272-16277.

22. **Li J, Wang X, Diaz J, Tsang SH, Buck CB, You J.** 2013. Merkel cell polyomavirus large T antigen disrupts host genomic integrity and inhibits cellular proliferation. J Virol **87:**9173-9188.

23. **Houben R, Shuda M, Weinkam R, Schrama D, Feng H, Chang Y, Moore PS, Becker JC.** 2010. Merkel cell polyomavirus-infected Merkel cell carcinoma cells require expression of viral T antigens. J Virol **84:**7064-7072.

24. **Shuda M, Kwun HJ, Feng H, Chang Y, Moore PS.** 2011. Human Merkel cell polyomavirus small T antigen is an oncoprotein targeting the 4E-BP1 translation regulator. J Clin Invest **121:**3623-3634.

25. **Liu W, Yang R, Payne AS, Schowalter RM, Spurgeon ME, Lambert PF, Xu X, Buck CB, You J.** 2016. Identifying the Target Cells and Mechanisms of Merkel Cell Polyomavirus Infection. Cell Host Microbe **19:**775-787.

26. **Liu W, Krump NA, MacDonald M, You J.** 2018. Merkel Cell Polyomavirus Infection of Animal Dermal Fibroblasts. J Virol **92**.

27. **Pastrana DV, Tolstov YL, Becker JC, Moore PS, Chang Y, Buck CB.** 2009. Quantitation of human seroresponsiveness to Merkel cell polyomavirus. PLoS Pathog **5:**e1000578.

887 28. **Schowalter RM, Pastrana DV, Buck CB.** 2011. Glycosaminoglycans and
888 sialylated glycans sequentially facilitate Merkel cell polyomavirus infectious
889 entry. PLoS Pathog **7:**e1002161.
890 29. **Schowalter RM, Reinhold WC, Buck CB.** 2012. Entry tropism of BK and
891 Merkel cell polyomaviruses in cell culture. PLoS One **7:**e42181.
892 30. **Neu U, Hengel H, Blaum BS, Schowalter RM, Macejak D, Gilbert M,**
893 **Wakarchuk WW, Imamura A, Ando H, Kiso M, Arnberg N, Garcea RL,**
894 **Peters T, Buck CB, Stehle T.** 2012. Structures of Merkel cell polyomavirus
895 VP1 complexes define a sialic acid binding site required for infection. PLoS
896 Pathog **8:**e1002738.
897 31. **Erickson KD, Garcea RL, Tsai B.** 2009. Ganglioside GT1b is a putative host
898 cell receptor for the Merkel cell polyomavirus. J Virol **83:**10275-10279.
899 32. **Mercer J, Schelhaas M, Helenius A.** 2010. Virus entry by endocytosis. Annu
900 Rev Biochem **79:**803-833.
901 33. **Doherty GJ, McMahon HT.** 2009. Mechanisms of endocytosis. Annu Rev
902 Biochem **78:**857-902.
903 34. **Anderson HA, Chen Y, Norkin LC.** 1996. Bound simian virus 40 translocates
904 to caveolin-enriched membrane domains, and its entry is inhibited by drugs
905 that selectively disrupt caveolae. Mol Biol Cell **7:**1825-1834.
906 35. **Parton RG, Richards AA.** 2003. Lipid rafts and caveolae as portals for
907 endocytosis: new insights and common mechanisms. Traffic **4:**724-738.
908 36. **Pelkmans L, Kartenbeck J, Helenius A.** 2001. Caveolar endocytosis of
909 simian virus 40 reveals a new two-step vesicular-transport pathway to the ER.
910 Nat Cell Biol **3:**473-483.
911 37. **Norkin LC, Anderson HA, Wolfrom SA, Oppenheim A.** 2002. Caveolar
912 endocytosis of simian virus 40 is followed by brefeldin A-sensitive transport to

913 the endoplasmic reticulum, where the virus disassembles. J Virol **76:**5156-
914 5166.
915 38. **Pho MT, Ashok A, Atwood WJ.** 2000. JC virus enters human glial cells by
916 clathrin-dependent receptor-mediated endocytosis. J Virol **74:**2288-2292.
917 39. **Dupzyk A, Tsai B.** 2016. How Polyomaviruses Exploit the ERAD Machinery
918 to Cause Infection. Viruses **8:**242.
919 40. **Schelhaas M, Malmstrom J, Pelkmans L, Haugstetter J, Ellgaard L,**
920 **Grunewald K, Helenius A.** 2007. Simian Virus 40 depends on ER protein
921 folding and quality control factors for entry into host cells. Cell **131:**516-529.
922 41. **Inoue T, Tsai B.** 2015. A nucleotide exchange factor promotes endoplasmic
923 reticulum-to-cytosol membrane penetration of the nonenveloped virus simian
924 virus 40. J Virol **89:**4069-4079.
925 42. **Geiger R, Andritschke D, Friebe S, Herzog F, Luisoni S, Heger T,**
926 **Helenius A.** 2011. BAP31 and BiP are essential for dislocation of SV40 from
927 the endoplasmic reticulum to the cytosol. Nat Cell Biol **13:**1305-1314.
928 43. **Walczak CP, Tsai B.** 2011. A PDI family network acts distinctly and
929 coordinately with ERp29 to facilitate polyomavirus infection. J Virol **85:**2386-
930 2396.
931 44. **Helenius A, Kartenbeck J, Simons K, Fries E.** 1980. On the entry of Semliki
932 forest virus into BHK-21 cells. J Cell Biol **84:**404-420.
933 45. **Schelhaas M, Shah B, Holzer M, Blattmann P, Kuhling L, Day PM, Schiller**
934 **JT, Helenius A.** 2012. Entry of human papillomavirus type 16 by actin-
935 dependent, clathrin- and lipid raft-independent endocytosis. PLoS Pathog
936 **8:**e1002657.
937 46. **Kuhling L, Schelhaas M.** 2014. Systematic analysis of endocytosis by
938 cellular perturbations. Methods Mol Biol **1174:**19-46.

939 47. **Boron WF, De Weer P.** 1976. Intracellular pH transients in squid giant axons
940 caused by CO2, NH3, and metabolic inhibitors. J Gen Physiol **67:**91-112.
941 48. **Engel S, Heger T, Mancini R, Herzog F, Kartenbeck J, Hayer A, Helenius**
942 **A.** 2011. Role of endosomes in simian virus 40 entry and infection. J Virol
943 **85:**4198-4211.
944 49. **Braakman I, Helenius J, Helenius A.** 1992. Manipulating disulfide bond
945 formation and protein folding in the endoplasmic reticulum. EMBO J **11:**1717-
946 1722.
947 50. **Safaiyan F, Kolset SO, Prydz K, Gottfridsson E, Lindahl U, Salmivirta M.**
948 1999. Selective effects of sodium chlorate treatment on the sulfation of
949 heparan sulfate. J Biol Chem **274:**36267-36273.
950 51. **Cerqueira C, Liu Y, Kuhling L, Chai W, Hafezi W, van Kuppevelt TH, Kuhn**
951 **JE, Feizi T, Schelhaas M.** 2013. Heparin increases the infectivity of Human
952 Papillomavirus type 16 independent of cell surface proteoglycans and induces
953 L1 epitope exposure. Cell Microbiol **15:**1818-1836.
954 52. **Weis W, Brown JH, Cusack S, Paulson JC, Skehel JJ, Wiley DC.** 1988.
955 Structure of the influenza virus haemagglutinin complexed with its receptor,
956 sialic acid. Nature **333:**426-431.
957 53. **von Kleist L, Stahlschmidt W, Bulut H, Gromova K, Puchkov D,**
958 **Robertson MJ, MacGregor KA, Tomilin N, Pechstein A, Chau N, Chircop**
959 **M, Sakoff J, von Kries JP, Saenger W, Krausslich HG, Shupliakov O,**
960 **Robinson PJ, McCluskey A, Haucke V.** 2011. Role of the clathrin terminal
961 domain in regulating coated pit dynamics revealed by small molecule
962 inhibition. Cell **146:**471-484.
963 54. **Doxsey SJ, Brodsky FM, Blank GS, Helenius A.** 1987. Inhibition of
964 endocytosis by anti-clathrin antibodies. Cell **50:**453-463.

965 55. **Macia E, Ehrlich M, Massol R, Boucrot E, Brunner C, Kirchhausen T.**
966 2006. Dynasore, a Cell-Permeable Inhibitor of Dynamin. Developmental Cell
967 **10:**839-850.
968 56. **Pelkmans L, Puntener D, Helenius A.** 2002. Local actin polymerization and
969 dynamin recruitment in SV40-induced internalization of caveolae. Science
970 **296:**535-539.
971 57. **Neufeld EB, Cooney AM, Pitha J, Dawidowicz EA, Dwyer NK, Pentchev**
972 **PG, Blanchette-Mackie EJ.** 1996. Intracellular Trafficking of Cholesterol
973 Monitored with a Cyclodextrin. Journal of Biological Chemistry **271:**21604-
974 21613.
975 58. **Rothberg KG, Heuser JE, Donzell WC, Ying Y-S, Glenney JR, Anderson**
976 **RGW.** 1992. Caveolin, a protein component of caveolae membrane coats. Cell
977 **68:**673-682.
978 59. **Metherall JE, Waugh K, Li H.** 1996. Progesterone Inhibits Cholesterol
979 Biosynthesis in Cultured Cells: ACCUMULATION OF CHOLESTEROL
980 PRECURSORS. Journal of Biological Chemistry **271:**2627-2633.
981 60. **Koivusalo M, Welch C, Hayashi H, Scott CC, Kim M, Alexander T, Touret**
982 **N, Hahn KM, Grinstein S.** 2010. Amiloride inhibits macropinocytosis by
983 lowering submembranous pH and preventing Rac1 and Cdc42 signaling. J
984 Cell Biol **188:**547-563.
985 61. **L'Allemain G, Paris S, Pouyssegur J.** 1984. Growth factor action and
986 intracellular pH regulation in fibroblasts. Evidence for a major role of the
987 Na+/H+ antiport. J Biol Chem **259:**5809-5815.
988 62. **Brown SS, Spudich JA.** 1979. Cytochalasin inhibits the rate of elongation of
989 actin filament fragments. The Journal of cell biology **83:**657-662.

990 63. **Bubb MR, Senderowicz AM, Sausville EA, Duncan KL, Korn ED.** 1994.
991 Jasplakinolide, a cytotoxic natural product, induces actin polymerization and
992 competitively inhibits the binding of phalloidin to F-actin. The Journal of
993 biological chemistry **269**.
994 64. **Niedergang F, Chavrier P.** 2005. Regulation of phagocytosis by Rho
995 GTPases. Curr Top Microbiol Immunol **291:**43-60.
996 65. **Mercer J, Helenius A.** 2009. Virus entry by macropinocytosis. Nat Cell Biol
997 **11:**510-520.
998 66. **Just I, Fritz G, Aktories K, Giry M, Popoff MR, Boquet P, Hegenbarth S,**
999 **von Eichel-Streiber C.** 1994. Clostridium difficile toxin B acts on the GTP-
1000 binding protein Rho. J Biol Chem **269:**10706-10712.
1001 67. **Akiyama T, Ishida J, Nakagawa S, Ogawara H, Watanabe S, Itoh N,**
1002 **Shibuya M, Fukami Y.** 1987. Genistein, a specific inhibitor of tyrosine-specific
1003 protein kinases. J Biol Chem **262:**5592-5595.
1004 68. **Gordon JA.** 1991. Use of vanadate as protein-phosphotyrosine phosphatase
1005 inhibitor. Methods in Enzymology **201:**477-482.
1006 69. **Huyer G, Liu S, Kelly J, Moffat J, Payette P, Kennedy B, Tsaprailis G,**
1007 **Gresser MJ, Ramachandran C.** 1997. Mechanism of Inhibition of Protein-
1008 tyrosine Phosphatases by Vanadate and Pervanadate. Journal of Biological
1009 Chemistry **272:**843-851.
1010 70. **Bialojan C, Takai A.** 1988. Inhibitory effect of a marine-sponge toxin, okadaic
1011 acid, on protein phosphatases. Specificity and kinetics. Biochem J **256:**283-
1012 290.
1013 71. **Yoshimori T, Yamamoto A, Moriyamas Y, Futais M, Tashiroq Y.** 1991.
1014 Bafilomycin AI, a Specific Inhibitor of Vacuolar-type H + -ATPase , Inhibits

Acidification and Protein Degradation in Lysosomes of Cultured Cells. The Journal of biological chemistry.

72. **Stebbings H.** 1995. Microtubule-based intracellular transport of organelles. **2:**113-140.

73. **Cheung HT, Terry DS.** 1980. Effects of nocodazole, a new synthetic microtubule inhibitor, on movement and spreading of mouse peritoneal macrophages. Cell Biol Int Rep **4:**1125-1129.

74. **Fujiwara T, Oda K, Yokota S, Takatsuki A, Ikehara Y.** 1988. Brefeldin A causes disassembly of the Golgi complex and accumulation of secretory proteins in the endoplasmic reticulum. J Biol Chem **263:**18545-18552.

75. **Clever J, Yamada M, Kasamatsu H.** 1991. Import of simian virus 40 virions through nuclear pore complexes. Proc Natl Acad Sci U S A **88:**7333-7337.

76. **Pyeon D, Pearce SM, Lank SM, Ahlquist P, Lambert PF.** 2009. Establishment of human papillomavirus infection requires cell cycle progression. PLoS Pathog **5:**e1000318.

77. **Aydin I, Weber S, Snijder B, Samperio Ventayol P, Kuhbacher A, Becker M, Day PM, Schiller JT, Kann M, Pelkmans L, Helenius A, Schelhaas M.** 2014. Large scale RNAi reveals the requirement of nuclear envelope breakdown for nuclear import of human papillomaviruses. PLoS Pathog **10:**e1004162.

78. **Spadari S, Sala F, Pedrali-Noy G.** 1982. Aphidicolin: a specific inhibitor of nuclear DNA replication in eukaryotes. Trends in Biochemical Sciences **7:**29-32.

79. **Froshauer S, Kartenbeck J, Helenius A.** 1988. Alphavirus RNA replicase is located on the cytoplasmic surface of endosomes and lysosomes. The Journal of Cell Biology **107:**2075-2086.

80. **Ewers H, Romer W, Smith AE, Bacia K, Dmitrieff S, Chai W, Mancini R, Kartenbeck J, Chambon V, Berland L, Oppenheim A, Schwarzmann G, Feizi T, Schwille P, Sens P, Helenius A, Johannes L.** 2010. GM1 structure determines SV40-induced membrane invagination and infection. Nat Cell Biol **12:**11-18; sup pp 11-12.

81. **Kartenbeck J, Stukenbrok H, Helenius A.** 1989. Endocytosis of simian virus 40 into the endoplasmic reticulum. J Cell Biol **109:**2721-2729.

82. **Kirkham M, Fujita A, Chadda R, Nixon SJ, Kurzchalia TV, Sharma DK, Pagano RE, Hancock JF, Mayor S, Parton RG.** 2005. Ultrastructural identification of uncoated caveolin-independent early endocytic vehicles. J Cell Biol **168:**465-476.

83. **Sabharanjak S, Sharma P, Parton RG, Mayor S.** 2002. GPI-anchored proteins are delivered to recycling endosomes via a distinct cdc42-regulated, clathrin-independent pinocytic pathway. Dev Cell **2:**411-423.

84. **Bennett SM, Jiang M, Imperiale MJ.** 2013. Role of cell-type-specific endoplasmic reticulum-associated degradation in polyomavirus trafficking. J Virol **87:**8843-8852.

85. **Nelson CD, Derdowski A, Maginnis MS, O'Hara BA, Atwood WJ.** 2012. The VP1 subunit of JC polyomavirus recapitulates early events in viral trafficking and is a novel tool to study polyomavirus entry. Virology **428:**30-40.

86. **Querbes W, O'Hara BA, Williams G, Atwood WJ.** 2006. Invasion of host cells by JC virus identifies a novel role for caveolae in endosomal sorting of noncaveolar ligands. J Virol **80:**9402-9413.

87. **Blaum BS, Neu U, Peters T, Stehle T.** 2018. Spin ballet for sweet encounters: saturation-transfer difference NMR and X-ray crystallography

complement each other in the elucidation of protein-glycan interactions. Acta Crystallogr F Struct Biol Commun **74:**451-462.

88. **Geoghegan EM, Pastrana DV, Schowalter RM, Ray U, Gao W, Ho M, Pauly GT, Sigano DM, Kaynor C, Cahir-McFarland E, Combaluzier B, Grimm J, Buck CB.** 2017. Infectious Entry and Neutralization of Pathogenic JC Polyomaviruses. Cell Rep **21:**1169-1179.

89. **Neu U, Maginnis MS, Palma AS, Stroh LJ, Nelson CD, Feizi T, Atwood WJ, Stehle T.** 2010. Structure-function analysis of the human JC polyomavirus establishes the LSTc pentasaccharide as a functional receptor motif. Cell Host Microbe **8:**309-319.

90. **Tsai B, Gilbert JM, Stehle T, Lencer W, Benjamin TL, Rapoport TA.** 2003. Gangliosides are receptors for murine polyoma virus and SV40. EMBO J **22:**4346-4355.

91. **Payne CK, Jones SA, Chen C, Zhuang X.** 2007. Internalization and trafficking of cell surface proteoglycans and proteoglycan-binding ligands. Traffic **8:**389-401.

92. **Sarrazin S, Lamanna WC, Esko JD.** 2011. Heparan sulfate proteoglycans. Cold Spring Harb Perspect Biol **3**.

93. **Qian M, Cai D, Verhey KJ, Tsai B.** 2009. A lipid receptor sorts polyomavirus from the endolysosome to the endoplasmic reticulum to cause infection. PLoS Pathog **5:**e1000465.

94. **Cerqueira C, Samperio Ventayol P, Vogeley C, Schelhaas M.** 2015. Kallikrein-8 proteolytically processes Human papillomaviruses in the extracellular space to facilitate entry into host cells. J Virol doi:10.1128/JVI.00234-15.

95. **Aderem A, Underhill DM.** 1999. Mechanisms of phagocytosis in macrophages. Annu Rev Immunol **17:**593-623.

96. **Lamaze C, Dujeancourt A, Baba T, Lo CG, Benmerah A, Dautry-Varsat A.** 2001. Interleukin 2 receptors and detergent-resistant membrane domains define a clathrin-independent endocytic pathway. Mol Cell **7:**661-671.

97. **Pelkmans L, Burli T, Zerial M, Helenius A.** 2004. Caveolin-stabilized membrane domains as multifunctional transport and sorting devices in endocytic membrane traffic. Cell **118:**767-780.

98. **Liebl D, Difato F, Hornikova L, Mannova P, Stokrova J, Forstova J.** 2006. Mouse polyomavirus enters early endosomes, requires their acidic pH for productive infection, and meets transferrin cargo in Rab11-positive endosomes. J Virol **80:**4610-4622.

99. **Eash S, Querbes W, Atwood WJ.** 2004. Infection of vero cells by BK virus is dependent on caveolae. J Virol **78:**11583-11590.

100. **Aydin I, Villalonga-Planells R, Greune L, Bronnimann MP, Calton CM, Becker M, Lai KY, Campos SK, Schmidt MA, Schelhaas M.** 2017. A central region in the minor capsid protein of papillomaviruses facilitates viral genome tethering and membrane penetration for mitotic nuclear entry. PLoS Pathog **13:**e1006308.

101. **Nakanishi A, Clever J, Yamada M, Li PP, Kasamatsu H.** 1996. Association with capsid proteins promotes nuclear targeting of simian virus 40 DNA. Proc Natl Acad Sci U S A **93:**96-100.

102. **Nakanishi A, Shum D, Morioka H, Otsuka E, Kasamatsu H.** 2002. Interaction of the Vp3 nuclear localization signal with the importin alpha 2/beta heterodimer directs nuclear entry of infecting simian virus 40. J Virol **76:**9368-9377.

1117 103. **Nakanishi A, Li PP, Qu Q, Jafri QH, Kasamatsu H.** 2007. Molecular
1118 dissection of nuclear entry-competent SV40 during infection. Virus Res
1119 **124:**226-230.
1120 104. **Hanson PI, Cashikar A.** 2012. Multivesicular body morphogenesis. Annu Rev
1121 Cell Dev Biol **28:**337-362.
1122 105. **Buck CB, Pastrana DV, Lowy DR, Schiller JT.** 2005. Generation of HPV
1123 pseudovirions using transfection and their use in neutralization assays.
1124 Methods Mol Med **119:**445-462.
1125 106. **Buck CB, Thompson CD, Pang YY, Lowy DR, Schiller JT.** 2005. Maturation
1126 of papillomavirus capsids. J Virol **79:**2839-2846.
1127 107. **Cardone G, Moyer AL, Cheng N, Thompson CD, Dvoretzky I, Lowy DR,**
1128 **Schiller JT, Steven AC, Buck CB, Trus BL.** 2014. Maturation of the Human
1129 Papillomavirus 16 Capsid. mBio **5**.
1130 108. **Marsh M, Helenius A.** 1980. Adsorptive endocytosis of Semliki Forest virus. J
1131 Mol Biol **142:**439-454.
1132 109. **Samperio Ventayol P, Schelhaas M.** 2015. Fluorescently Labeled Human
1133 Papillomavirus Pseudovirions for Use in Virus Entry Experiments. Curr Protoc
1134 Microbiol **37:**14B 14 11-22.
1135 110. **Vonderheit A, Helenius A.** 2005. Rab7 associates with early endosomes to
1136 mediate sorting and transport of Semliki forest virus to late endosomes. PLoS
1137 Biol **3:**e233.
1138 111. **Buck CB, Thompson CD.** 2007. Production of papillomavirus-based gene
1139 transfer vectors. Curr Protoc Cell Biol **Chapter 26:**Unit 26 21.
1140

Figure 1

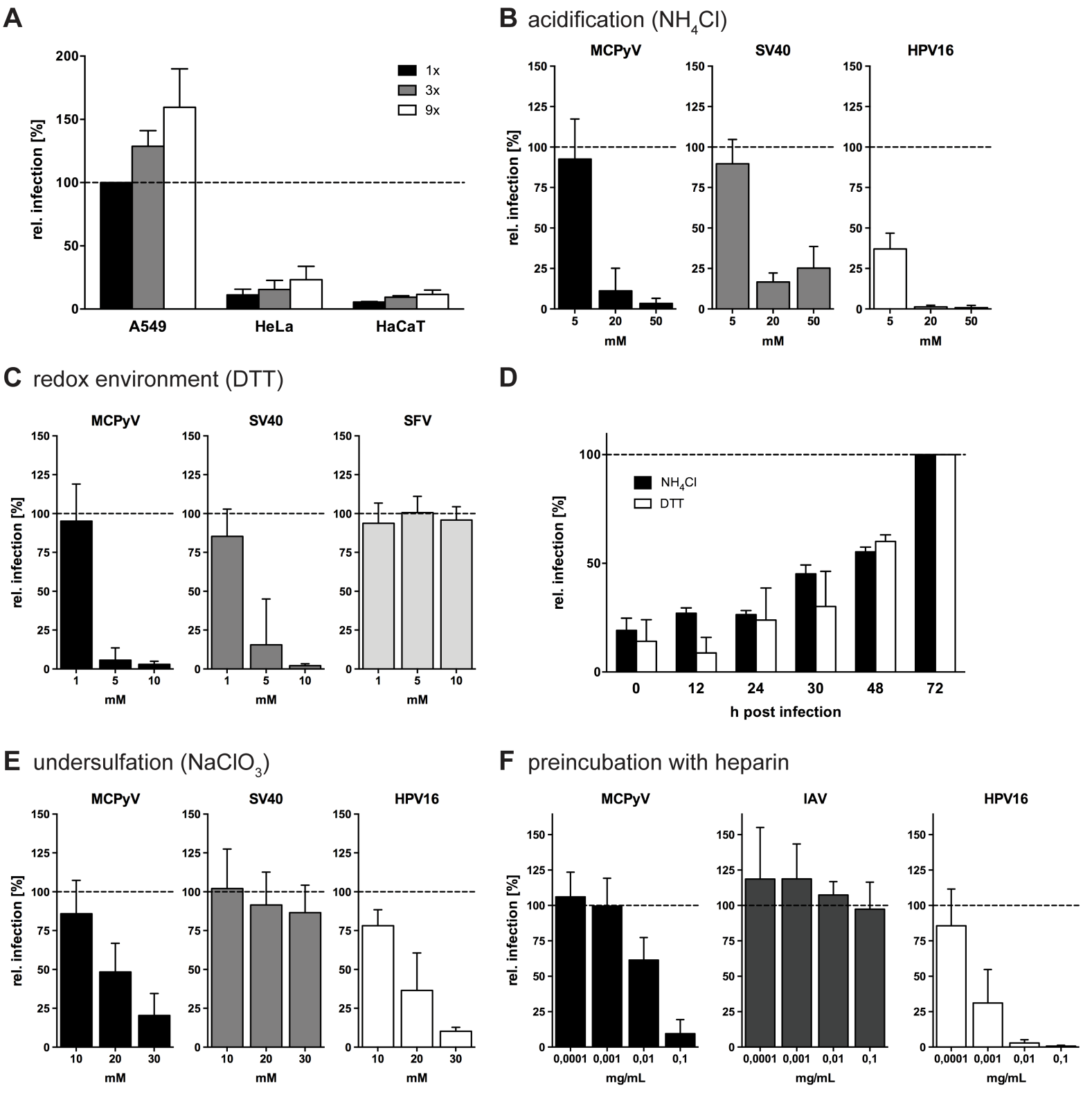
A
rel. infection [%]
1x
3x
9x
A549
HeLa
HaCaT
B acidification (NH_4Cl)
MCPyV
SV40
HPV16
mM
C redox environment (DTT)
MCPyV
SV40
SFV
mM
D
NH_4Cl
DTT
h post infection
E undersulfation ($NaClO_3$)
MCPyV
SV40
HPV16
mM
F preincubation with heparin
MCPyV
IAV
HPV16
mg/mL

Figure 2

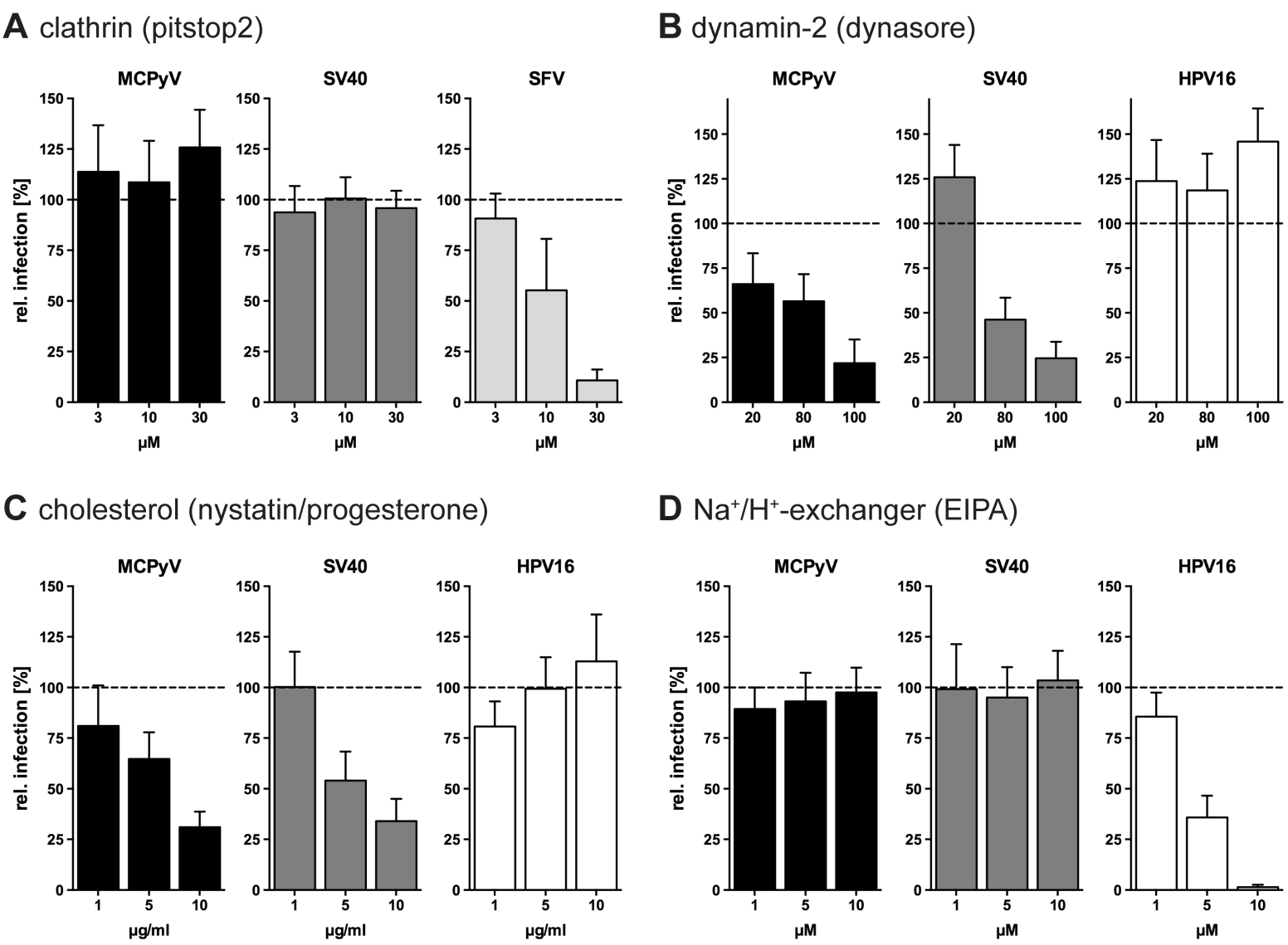
A clathrin (pitstop2)
MCPyV
SV40
SFV
rel. infection [%]
150
125
100
75
50
25
0
3
10
30
µM
B dynamin-2 (dynasore)
MCPyV
SV40
HPV16
20
80
100
µM
C cholesterol (nystatin/progesterone)
MCPyV
SV40
HPV16
1
5
10
µg/ml
D Na+/H+-exchanger (EIPA)
MCPyV
SV40
HPV16
µM

Figure 3

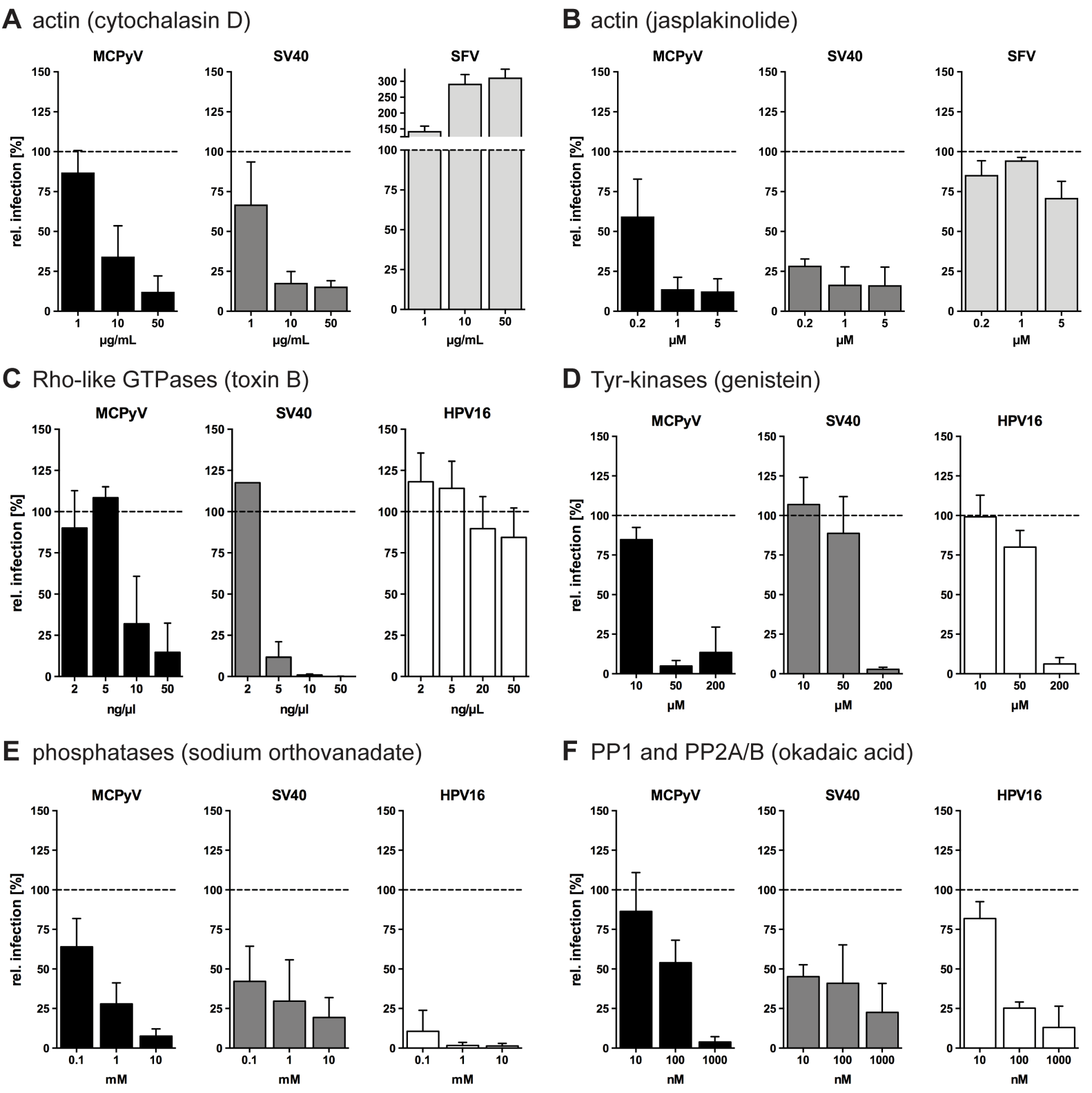
A actin (cytochalasin D)
MCPyV
SV40
SFV
rel. infection [%]
µg/mL
B actin (jasplakinolide)
µM
C Rho-like GTPases (toxin B)
HPV16
ng/µl
ng/µL
D Tyr-kinases (genistein)
E phosphatases (sodium orthovanadate)
mM
F PP1 and PP2A/B (okadaic acid)
nM

Figure 4

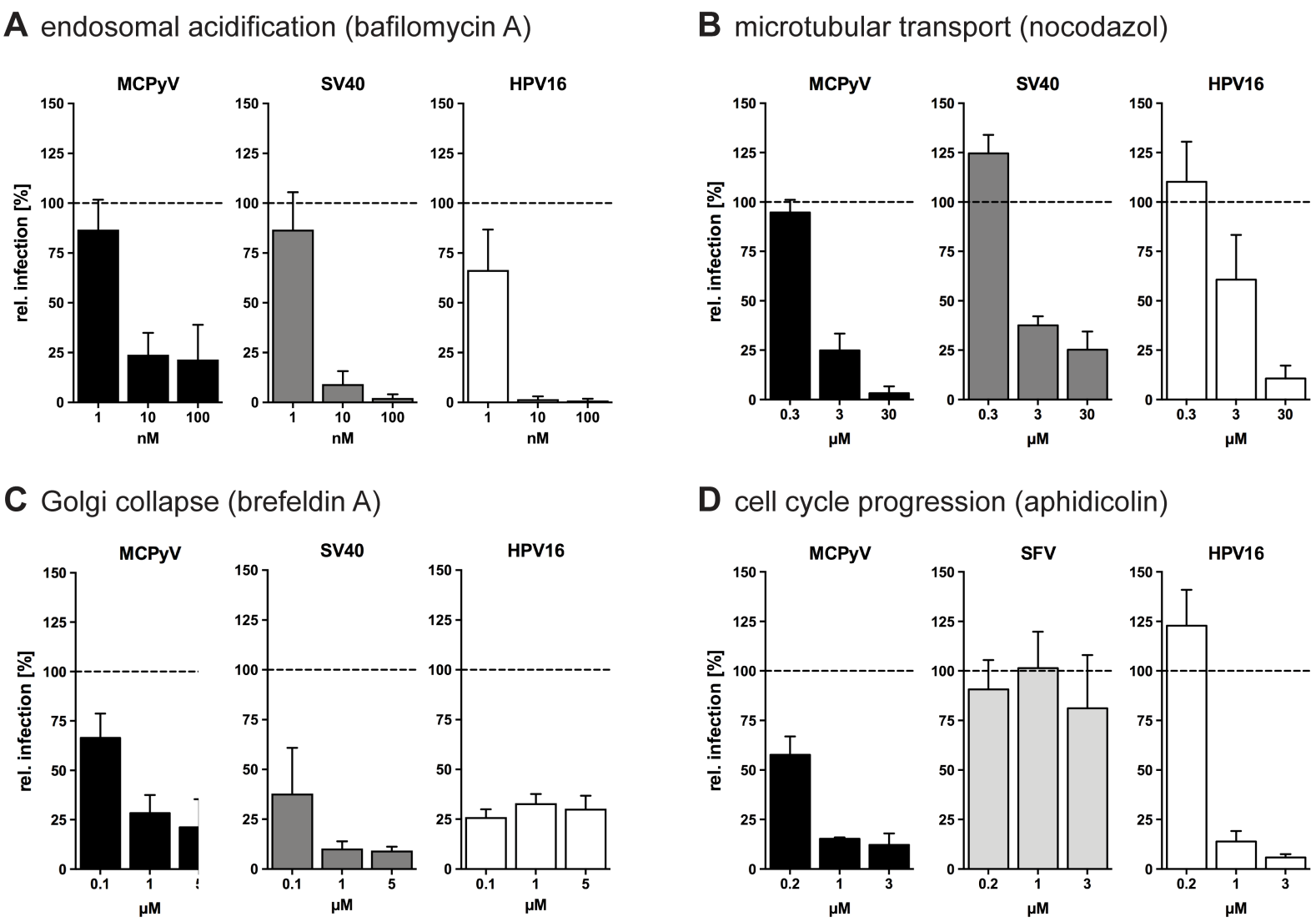
A endosomal acidification (bafilomycin A)
B microtubular transport (nocodazol)
C Golgi collapse (brefeldin A)
D cell cycle progression (aphidicolin)
MCPyV
SV40
HPV16
SFV
rel. infection [%]
nM
µM

Figure 5

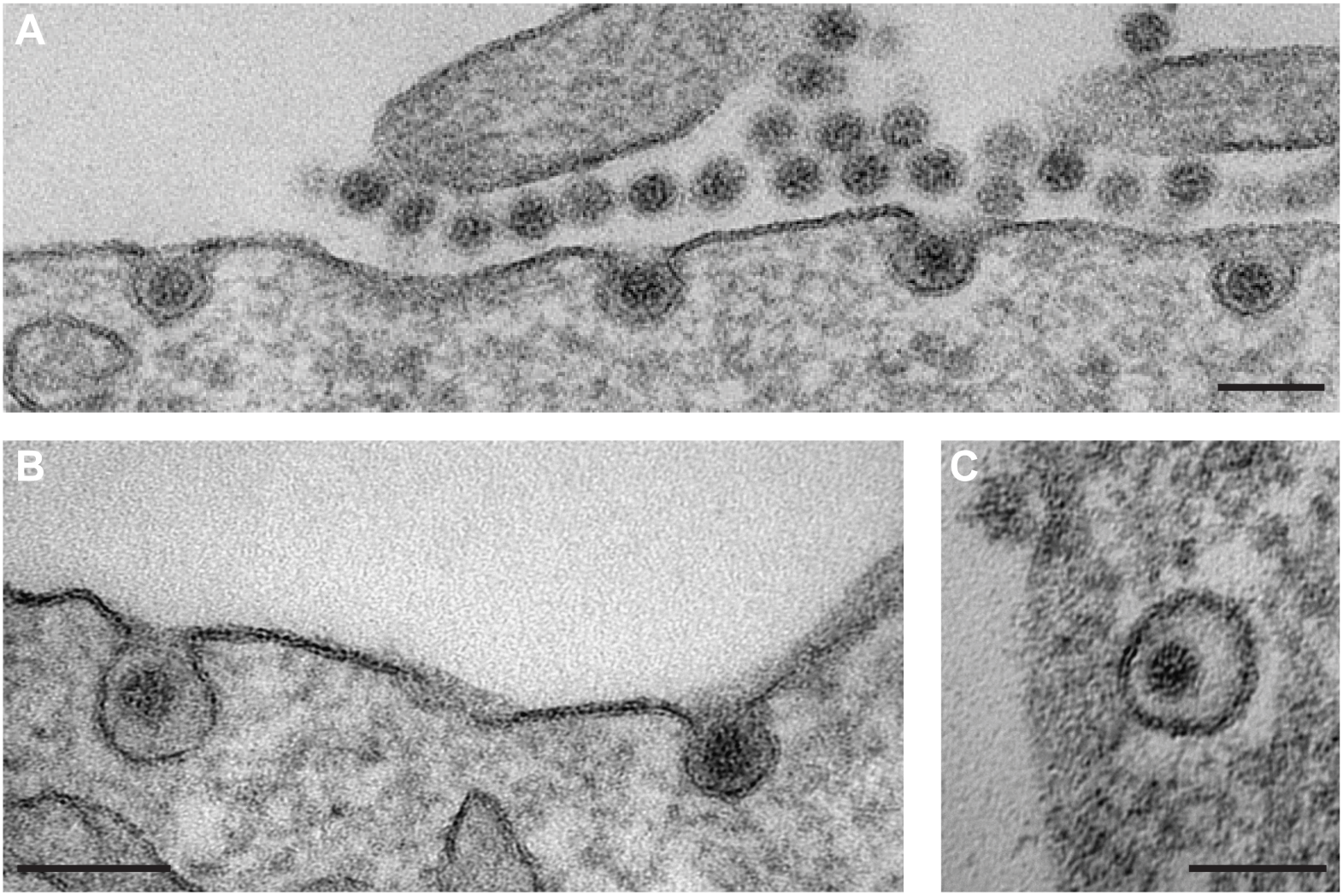

Figure 6

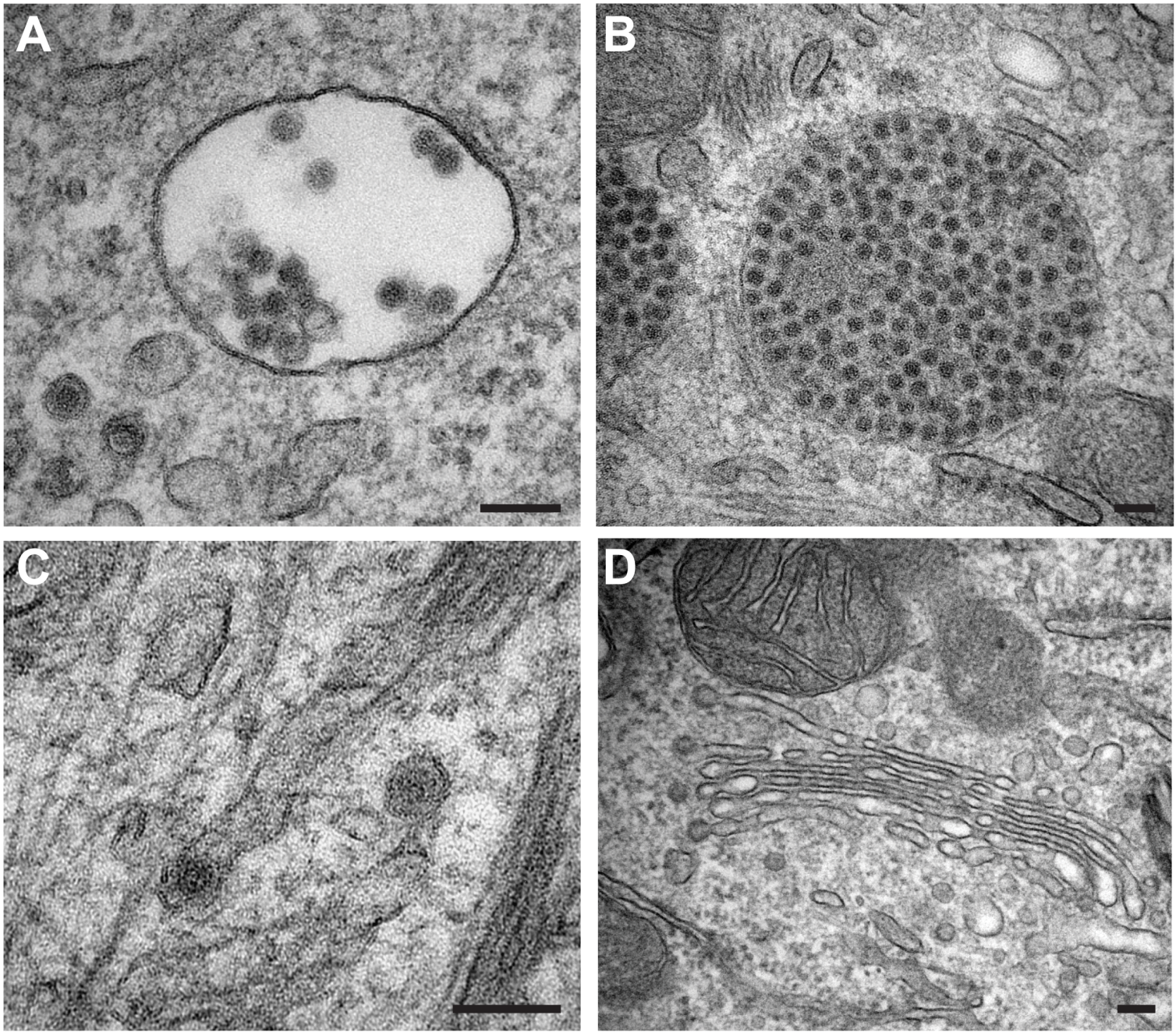

Figure 7

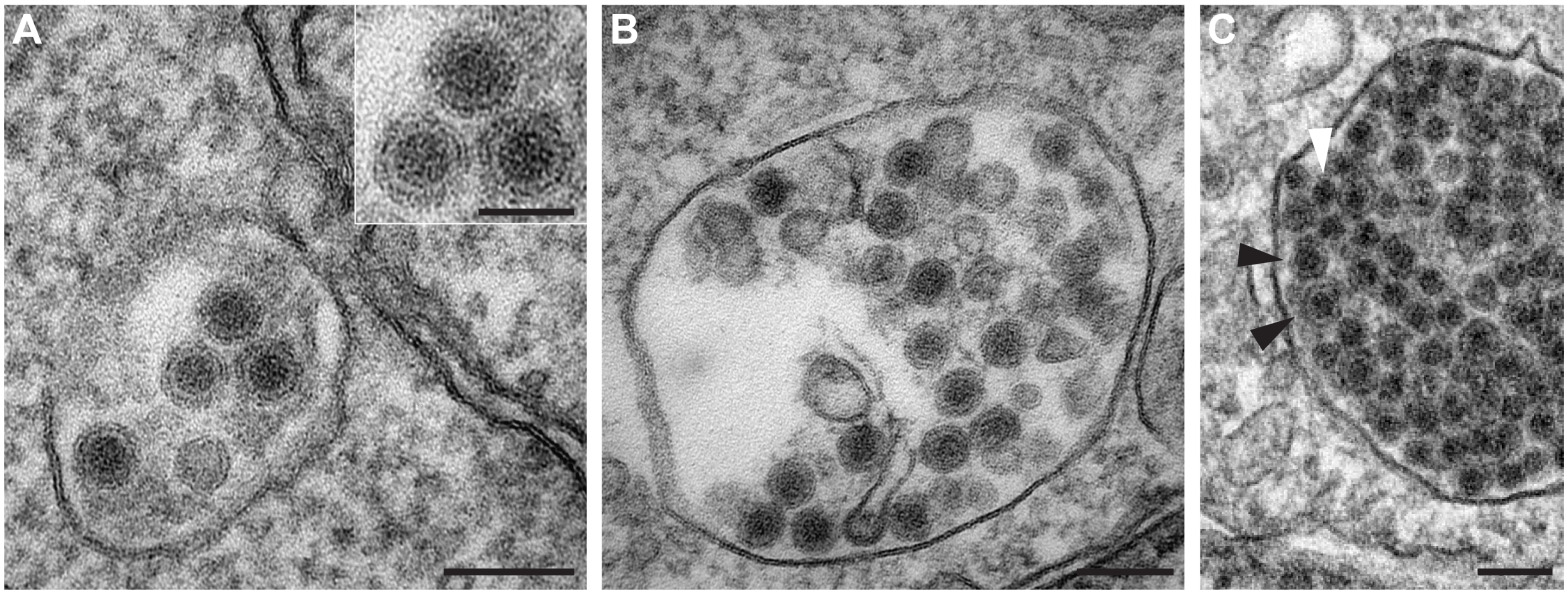

Figure 8

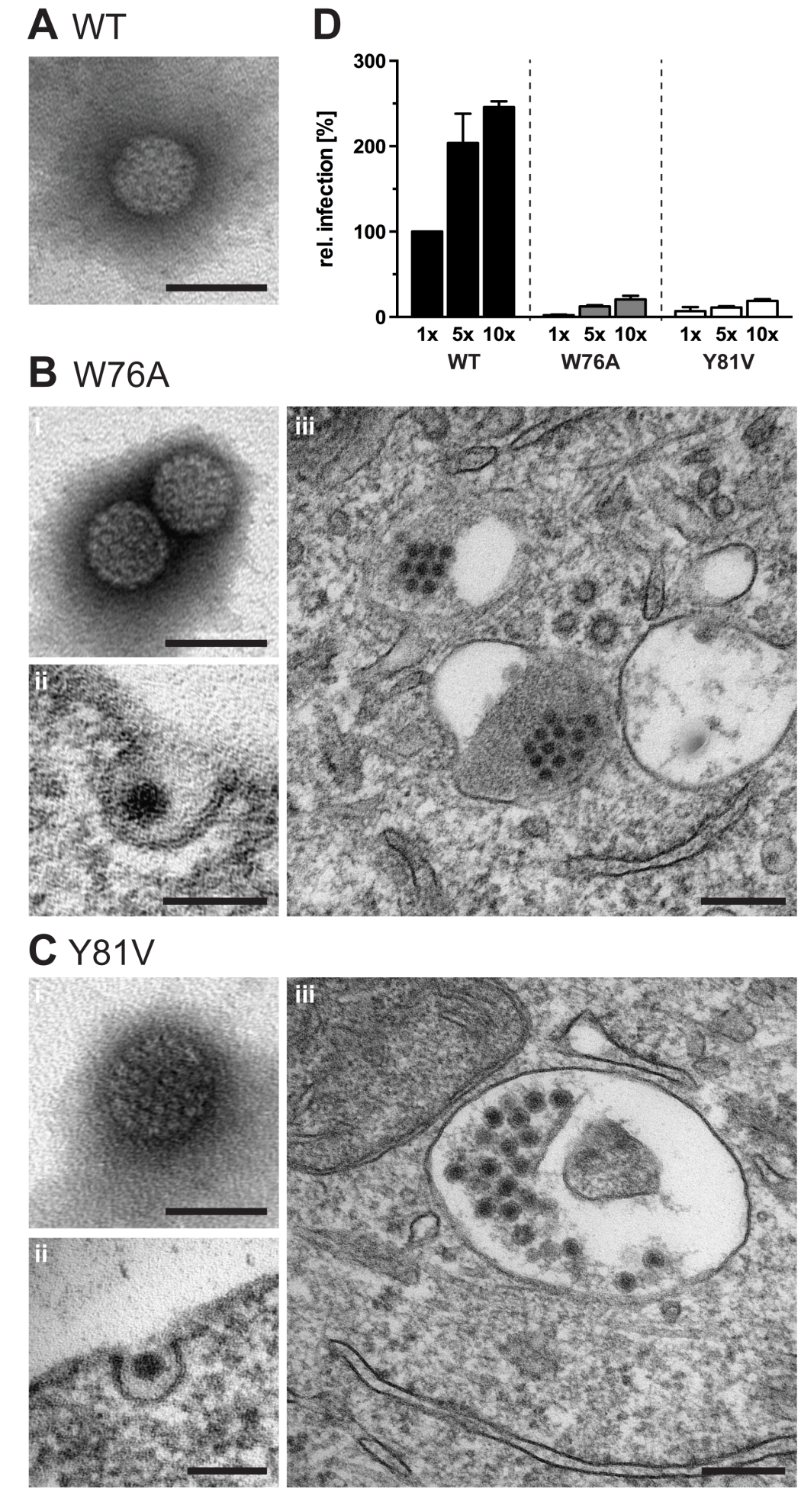
A WT
D
300
200
100
0
rel. infection [%]
1x 5x 10x
WT
1x 5x 10x
W76A
1x 5x 10x
Y81V
B W76A
i
ii
iii
C Y81V
i
ii
iii

Figure 9

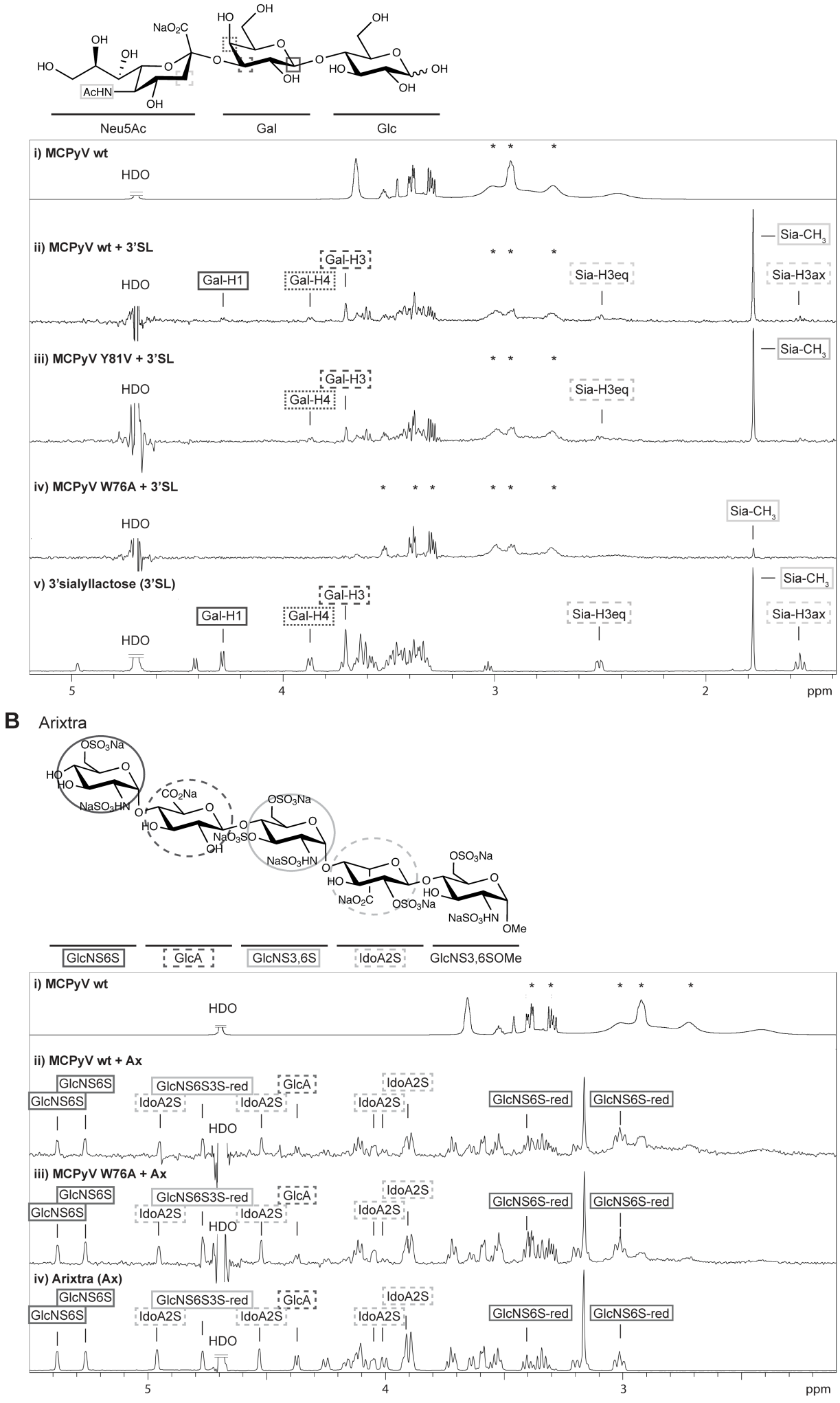
A
3'-Sialyllactose (Neu5Ac(α2-3)Gal(β1-4)Glc)
Neu5Ac
Gal
Glc
i) MCPyV wt
HDO
ii) MCPyV wt + 3'SL
Gal-H1
Gal-H4
Gal-H3
Sia-H3eq
Sia-H3ax
Sia-CH3
iii) MCPyV Y81V + 3'SL
iv) MCPyV W76A + 3'SL
v) 3'sialyllactose (3'SL)
5
4
3
2
ppm
B
Arixtra
GlcNS6S
GlcA
GlcNS3,6S
IdoA2S
GlcNS3,6SOMe
i) MCPyV wt
ii) MCPyV wt + Ax
GlcNS6S3S-red
GlcNS6S-red
iii) MCPyV W76A + Ax
iv) Arixtra (Ax)
5
4
3
ppm